J. metamorphic Geol., 2007, **25,** 953–974 doi:10.1111/j.1525-1314.2007.00737.x

Formation of eclogite, and reaction during exhumation to mid-crustal levels, Snowbird tectonic zone, western Canadian Shield

J. A. BALDWIN,[1] R. POWELL,[2] M. L. WILLIAMS[3] AND P. GONCALVES[4]
[1]*Department of Geosciences, University of Montana, Missoula, MT 59812-1296, USA (julie.baldwin@umontana.edu)*
[2]*School of Earth Sciences, The University of Melbourne, Melbourne, Vic. 3010, Australia*
[3]*Department of Geosciences, University of Massachusetts, Amherst, MA 01003, USA*
[4]*Department des Géosciences, Université de Franche-Comté, Besançon, France*

ABSTRACT A re-evaluation of the *P–T* history of eclogite within the East Athabasca granulite terrane of the Snowbird tectonic zone, northern Saskatchewan, Canada was undertaken. Using calculated pseudosections in combination with new garnet–clinopyroxene and zircon and rutile trace element thermometry, peak metamorphic conditions are constrained to ~16 kbar and 750 °C, followed by near-isothermal decompression to ~10 kbar. Associated with the eclogite are two types of occurrences of sapphirine-bearing rocks preserving a rich variety of reaction textures that allow examination of the retrograde history below 10 kbar. The first occurs as a 1–2 m zone adjacent to the eclogite body with a peak assemblage of garnet–kyanite–quartz interpreted to have formed during the eclogite facies metamorphism. Rims of orthopyroxene and plagioclase developed around garnet, and sapphirine–plagioclase and spinel–plagioclase symplectites developed around kyanite. The second variety of sapphirine-bearing rocks occurs in kyanite veins within the eclogite. The veins involve orthopyroxene, garnet and plagioclase layers spatially organized around a central kyanite layer that are interpreted to have formed following the eclogite facies metamorphism. The layering has itself been modified, with, in particular, kyanite being replaced by sapphirine–plagioclase, spinel–plagioclase and corundum–plagioclase symplectites, as well as the kyanite being replaced by sillimanite. Petrological modelling in the CFMAS system examining chemical potential gradients between kyanite and surrounding quartz indicates that these vein textures probably formed during further essentially isothermal decompression, ultimately reaching ~7 kbar and 750 °C. These results indicate that the final reaction in these rocks occurred at mid-crustal levels at upper amphibolite facies conditions. Previous geochronological and thermochronological constraints bracket the time interval of decompression to < 5–10 Myr, indicating that ~25 km of exhumation took place during this interval. This corresponds to minimum unroofing rates of ~2–5 mm year^{-1} following eclogite facies metamorphism, after which the rocks resided at mid-crustal levels for 80–100 Myr.

Key words: chemical potential; kyanite eclogite; reaction textures; sapphirine; Saskatchewan.

INTRODUCTION

Understanding mineral equilibria and interpreting *P–T* paths is fundamental to deciphering the range of physical processes that affect the formation and modification of the continental crust. Metamorphic rocks preserve a record of pressure, temperature, strain and interaction with fluids or melt in the crust through time. Decoding the clues that mineral assemblages provide is thus central to studies of the origin and evolution of the continental crust. Work in recent years has seen an increased interest in evaluating the mineral equilibria of deep crustal rocks, including terranes containing high-pressure granulite and eclogite facies rocks (e.g. O'Brien & Rötzler, 2003). Such exposures are generally rare, but where exhumed, afford the opportunity to examine the nature of tectonometamorphic events affecting the deep crust, including the interactions between magmatism, metamorphism and deformation resulting in mass and heat transfer through the crust.

Establishing the *P–T* paths of eclogite (*sensu lato*, referring to rocks dominated by garnet and sodic clinopyroxene) has commonly involved the application of the garnet–clinopyroxene thermometer to establish peak temperatures, combined with the jadeite–quartz–albite barometer to establish minimum pressures. The decompression path is generally constrained by the interpretation of reaction textures, where present, that developed during the retrograde evolution. Typical textures include diopsidic clinopyroxene–plagioclase symplectites after Na-clinopyroxene, orthopyroxene–plagioclase symplectites replacing clinopyroxene, and amphibole–plagioclase kelyphite textures after garnet.

Less common are retrograde textures that involve aluminous phases, such as sapphirine, spinel, and corundum, which may be associated with kyanite eclogites (Johansson & Möller, 1986; Carswell *et al.*, 1989; O'Brien, 1992; Liati & Seidel, 1994; Möller, 1999). Such textures should constrain a segment of the decompression path and are commonly interpreted as a granulite or amphibolite facies overprinting following decompression.

A powerful approach for placing rocks into the appropriate context of a *P–T* path involves calculated pseudosections, showing the *P–T* dependence of mineral assemblage in a particular bulk composition (e.g. Stipska & Powell, 2005a). For eclogites, a recently developed amphibole model allows an evaluation of the effect of H_2O availability on the resulting mineral assemblages (Dale *et al.*, 2005). This study utilizes this model in a *P–T–M*(H_2O) evaluation of eclogites from the Snowbird tectonic zone (STZ) in the western Canadian Shield. The metamorphic evolution of these rocks has been discussed by Baldwin *et al.* (2004) but is re-evaluated here using the calculated pseudosections, combined with new garnet–clinopyroxene, Ti-in-zircon and Zr-in-rutile thermometry, better constraining the peak thermal conditions of these rocks. We then investigate the associated sapphirine-bearing lithologies and present a new quantitative approach for understanding the development of complex reaction textures in these rocks, in terms of the control of superimposed chemical potentials and chemical potential gradients that developed during the decompression history. Applying calculated petrogenetic grids at fixed chemical potential affords the opportunity to place constraints on the *P–T* conditions preserved in the symplectite and corona textures. Integrating our petrological modelling results with existing geochronological data, it is concluded that the regional exhumation of these rocks occurred during an initial phase of rapid decompression, possibly in two stages, following eclogite facies metamorphism, after which the rocks resided at mid-crustal levels for *c.* 80–100 Myr before the terrane was ultimately exhumed.

This study demonstrates how calculated pseudosections, conventional thermobarometric data, new trace element thermometers and new petrogenetic grids that examine chemical potential gradients may be integrated in order to construct high-resolution *P–T* paths for complex metamorphic terranes. Such integrated approaches are necessary for obtaining the maximum amount of information from the textures and assemblages observed in deep crustal terranes.

GEOLOGICAL SETTING

The STZ is a 2800-km-long linear element in the horizontal gravity gradient map of the Canadian Shield that extends from the Canadian Cordillera north-east to Hudson Bay (Goodacre *et al.*, 1987). It occurs at the boundary between the Rae and Hearne domains of the western Churchill Province, an extensive region of Archean crust bounded by the 2.0–1.9 Ga Taltson-Thelon orogen to the north-west and the 1.85–1.80 Ga Trans-Hudson orogen to the south-east (Fig. 1) (Hoffman, 1988). In northern Saskatchewan, a well-exposed segment of the STZ has been described as the East Athabasca granulite terrane, and consists of anastamosing lower crustal high-grade granulite facies rocks (Hanmer, 1994, 1997; Hanmer *et al.*, 1995a,b) (Fig. 1). The East Athabasca region has been variably interpreted as a Paleoproterozoic suture (Hoffman,

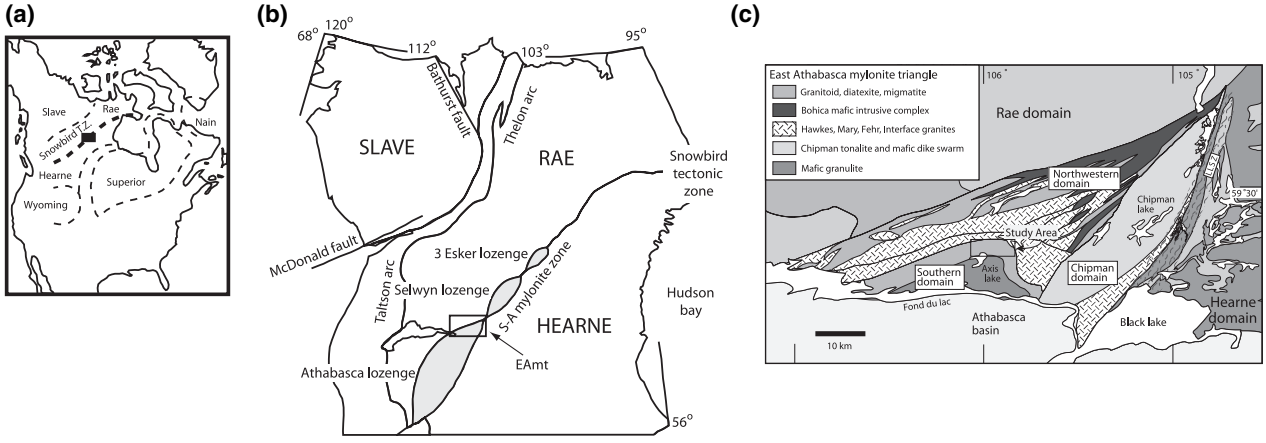

Fig. 1. (a) Map of North America showing the major Archean provinces and location of the Snowbird tectonic zone (STZ) along the heavy dashed line. Box shows location of the East Athabasca segment of the STZ. (b) Tectonic province map of the western Canadian Shield. The East Athabasca region occurs at the northern end of the Athabasca lozenge, one of three such features along the STZ. The central and southern portion of the Athabasca lozenge are covered by the Athabasca basin. Box outlines location of the East Athabasca mylonite triangle (EAmt). (c) Geological map of the EAmt showing major lithotectonic domains and location of the study area within the northern portion of the Southern domain. Eclogite and mafic granulite lenses occur within this unit, which is dominated by metaigneous high-*P* felsic granulites (garnet + kyanite + ternary feldspar). LLSZ = Legs Lake Shear Zone.

1988, 1989), an Archean intra-continental strike-slip shear zone (Hanmer, 1994; Hanmer *et al*., 1994, 1995a,b; Berman *et al*., 2000), and more recently as a complex feature resulting from the interaction of cross-cutting, hundred-km-scale, Paleoproterozoic shear zones, rather than from primary accretion (Mahan & Williams, 2005).

The East Athabasca granulite terrane exposes a broad area of high-pressure granulite facies rocks characterized by a highly segmented architecture, with discrete structural and lithological domains, each preserving distinct *P–T–t* histories (Fig. 1) (Snoeyenbos *et al*., 1995; Williams *et al*., 1995, 2000; Baldwin *et al*., 2003, 2004; Flowers *et al*., 2006a). The North-western domain is dominated by 2.6 Ga mafic and felsic plutonic rocks that record metamorphic conditions of ~10 kbar, 800 °C (Williams *et al*., 2000). The Chipman domain preserves a spectacular 1.9 Ga mafic dyke swarm that intruded a large tonalite gneiss body at 10–12 kbar and 750–850 °C (Williams *et al*., 1995; Flowers *et al*., 2006a). The Southern domain is the focus of this contribution. It contains both mafic and felsic granulites, as well as minor eclogite lenses that record higher pressure conditions of >15 kbar, >800 °C interpreted to have occurred at 1.9 Ga (Snoeyenbos *et al*., 1995; Baldwin *et al*., 2003, 2004, 2006). The eastern extent of the high-pressure rocks is marked by the Legs Lake shear zone (Fig. 1). The Hearne domain forms the footwall of this structure and records *P–T* conditions of 5 kbar and 600–700 °C, with regional exhumation of the deep crustal rocks at *c*. 1.85–1.80 Ga (Mahan *et al*., 2003, 2006b).

The Southern domain consists of three lithological units in varying proportions: felsic gneiss, mafic granulite and eclogite. The felsic gneiss, the most abundant lithology, is a garnetiferous quartzofeldspathic mylonitic gneiss (garnet + feldspar + quartz ± kyanite/sillimanite + rutile). The felsic gneiss is the dominant rock type in the northern portion of the Southern domain, and is interlayered with mafic granulite and eclogite lenses on a centimetre- to metre-scale. The southern portion of the Southern domain is dominated by mafic granulite (garnet + clinopyroxene + plagioclase + quartz ± orthopyroxene ± hornblende), and is interlayered with felsic gneiss similar to that found in the northern portion. *P–T–t* studies carried out on the three lithologies have constrained metamorphic conditions of >15 kbar, >800 °C (Snoeyenbos *et al*., 1995; Baldwin *et al*., 2003, 2004), and estimates of ≥1000 °C have been proposed for the felsic gneiss based on ternary feldspar thermometry (Snoeyenbos *et al*., 1995).

One of the controversies surrounding the Southern domain metamorphic evolution is the relative timing and relationship of metamorphic and magmatic events throughout the Archean and Paleoproterozoic. For example, accessory phases in the felsic gneiss record a complex growth history from >2.6 to 1.9 Ga (Baldwin *et al*., 2006). The oldest ages are interpreted to represent protolith crystallization ages. However, a notable population of *c*. 2.55 Ga zircon occurs in both the eclogite and mafic granulite lithologies which probably indicates an early metamorphic event, but the nature of this event is difficult to evaluate because of subsequent overprinting (Baldwin *et al*., 2003, 2004). The eclogite lithology contains a distinct population of metamorphic zircon that is 1904 Ma, which is interpreted to date the timing of high-*P* metamorphism (Baldwin *et al*., 2004). Previous interpretations have also linked this metamorphic event to extreme temperatures (>900–1000 °C) (e.g. Baldwin *et al*., 2004). However, it is important to note that the metamorphic temperatures in the Southern domain have been constrained by two methods that have serious inherent problems associated with them: ternary feldspar rehomogenization thermometry and garnet–clinopyroxene thermometry. The value of ternary feldspar thermometry for determining metamorphic conditions depends critically on the interpretation of metamorphic growth of the ternary feldspar. If such feldspar represents a relict igneous mineral then it contributes nothing about the metamorphic conditions (Stipska & Powell, 2005b). Garnet–clinopyroxene thermometry is much less precise than is commonly asserted because of uncertainties associated with, for example, the unknown content of Fe^{3+} in garnet and clinopyroxene (Proyer *et al*., 2004). Additionally, most workers commonly assume all Fe as Fe^{2+}, which strongly biases temperatures (and by association pressures) upwards (Stipska & Powell, 2005b).

Resolving the maximum metamorphic temperatures associated with the eclogite metamorphism in the Southern domain is crucial to understanding the petrogenesis of these rocks. In particular, the felsic gneiss has been proposed to represent the residue from a high-*T* melting event at high-*P*, producing the assemblage of garnet + kyanite + ternary feldspar (Snoeyenbos *et al*., 1995). This interpretation hinges on the ternary feldspar in the felsic gneiss being metamorphic in origin. Alternatively, ternary feldspar and garnet may have formed during igneous crystallization of a dry, high-*T* magma at, say 2.6 Ga, followed by kyanite formation during high-*P* metamorphism at 1.9 Ga. The refractory nature of the felsic gneiss may still result from, or be accentuated by, partial melting and melt loss but at lower temperatures (<800 °C). Given the ambiguity associated with determining the conditions of formation of the felsic gneisses, we focus attention on the eclogite itself.

As argued below, the high temperatures (>900 °C) obtained by garnet–clinopyroxene thermometry of the interlayered mafic granulite and eclogite lenses that have previously been reported by Baldwin *et al*. (2003, 2004) appear to overestimate the metamorphic conditions achieved in the Southern domain, resulting in misinterpretation of the metamorphic evolution, acknowledging the complication that in some instances higher temperatures may record igneous protolith

crystallization temperatures. This study aims to better constrain the maximum thermal conditions achieved in the Southern domain during Paleoproterozoic high-*P* metamorphism and place constraints on the decompression history of these rocks based on a re-assessment of the *P–T* history of eclogite, and new petrological descriptions and interpretation of associated sapphirine-bearing rocks that constrain the youngest segment of the *P–T* path preserved in the mineral assemblages.

ECLOGITE *P–T* EVOLUTION

Garnet–clinopyroxene thermometry

It is well known that the garnet–clinopyroxene Fe–Mg exchange thermometer is highly sensitive to mineral composition (e.g. ferric iron in clinopyroxene) such that a thermometer that does not take account of this may yield erroneous results. The Krogh Ravna (2000) calibration is used here for a reassessment of garnet–clinopyroxene temperatures. It is based on all the currently available experimental data, as well as some natural data, and supercedes previous calibrations.

Uncertainties on garnet–clinopyroxene temperatures are generally underestimated, related to the inherent sensitivity of such an exchange thermometer as the entropy of reaction is small. As a consequence, the contribution to the uncertainty arising from the difficulty in estimating ferric iron is large (Krogh Ravna & Terry, 2004). The common practice of assuming no ferric iron in clinopyroxene does remove the variability introduced, but it strongly biases the calculated temperature upwards. The approach presented here is the same as that followed by Stipska & Powell (2005a), using the methodology outlined in Carson & Powell (1997). This approach specifies a certain conversion of FeO to Fe_2O_3, which is then used to modify the original analysis so that it is stoichiometric and charge balanced for this value of ferric iron (see Stipska & Powell, 2005a). Combined calibration uncertainties and uncertainties in ferric estimation result in minimum errors on temperatures of $\sim \pm 80$ °C, a point that is not commonly acknowledged in most applications of the thermometer (Krogh Ravna, 2000).

The detailed petrology of eclogite in the Southern domain has been described by Baldwin *et al.* (2004), who took a traditional approach to calculating pressures and temperatures using the garnet–clinopyroxene thermometer calibration of Powell (1985) and the albite–jadeite–quartz barometer of Holland (1980). Temperatures were estimated in the range of 920–1000 °C with corresponding pressures of 18–20 kbar. As well as the problems relating to Fe^{3+} in the clinopyroxene alluded to above, and acknowledging that Powell (1985) tended to bias temperature upwards, additional care is required as much of the Na-clinopyroxene in these samples is modified by reaction to diopsidic clinopyroxene and sodic plagioclase.

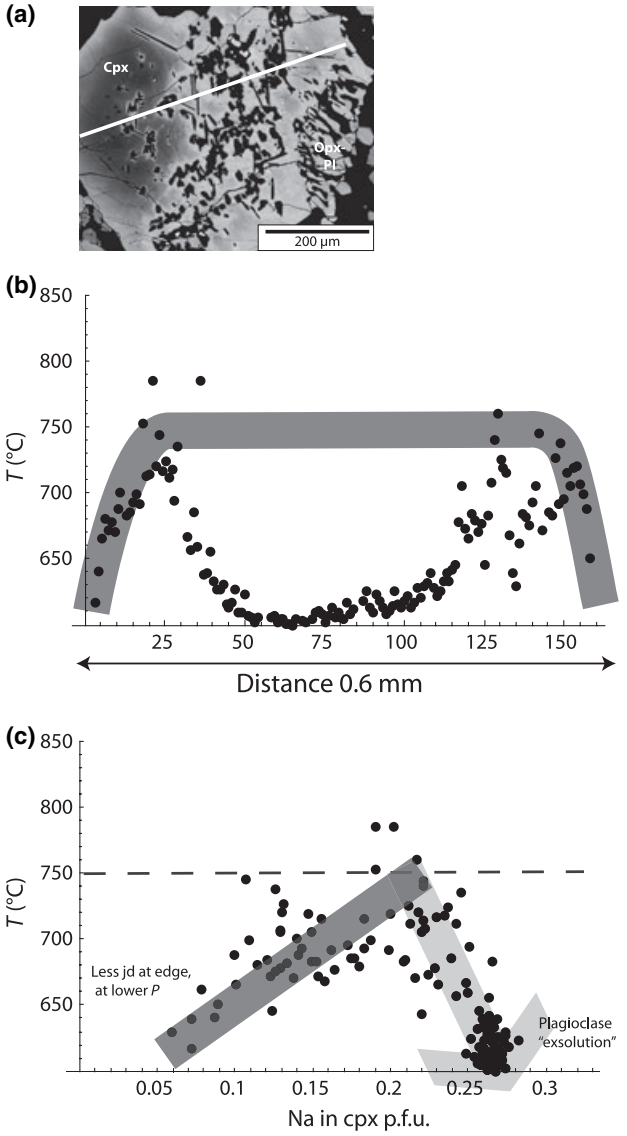

Fig. 2. (a) Backscattered electron image of clinopyroxene from sample 01SZ40b showing location of electron microprobe traverse. The left-hand side of the grain is dominated by plagioclase-free Na-rich clinopyroxene with maximum X_{Jd} of 0.23. The middle and right-hand side of the grain show extensive exsolution of plagioclase resulting in a less Na-rich diopsidic cpx. The right-hand edge of the grain is replaced by an opx–pl symplectite. (b) Plot of garnet–clinopyroxene temperatures calculated along the traverse shown in (a). The bold grey line shows the inferred original temperature profile prior to plagioclase exsolution. Spuriously low temperatures are preserved in the exsolution region. Rims are modified by diffusional re-equilibration. (c) Plot of temperature *v.* Na in cpx [(Na/(Na + Ca)]. The least jadeite-rich cpx occurs at the rim with the highest values recorded by the plagioclase exsolution region.

Figure 2(a) shows a backscattered electron image of one such grain, where the left-hand side preserves an area of relatively sodic clinopyroxene (Jd_{23}), whereas the right-hand side has reacted to diopsidic clinopyroxene and sodic plagioclase ($An_{29–44}$). A traverse

across this grain for calculated garnet–clinopyroxene temperatures using Krogh Ravna (2000) and the best analysis approach of Carson & Powell (1997) shows maximum temperatures of 750–800 °C, with anomalously low temperatures at the rim and within the area of the grain with symplectite formation. The inferred temperature profile of the grain is shown in Fig. 2(b) assuming that all clinopyroxene grains were in equilibrium with garnet, at a pressure of 16 kbar. Rims of clinopyroxene are devoid of plagioclase and preserve a lower jadeite content, most probably reflecting re-equilibration, possibly with garnet, along the retrograde path. The area of symplectite formation is likely not to have equilibrated with garnet, so thus give spurious temperatures. Maximum jadeite contents from more Na-rich areas preserve the highest temperatures, which have been calculated at 700–800 °C for the range of samples presented in Baldwin *et al*. (2004). The grains typically show a steady increase in jadeite content from rim to core, with the areas of plagioclase exsolution from clinopyroxene preserving higher Na/(Na + Ca) values (Fig. 2c).

The interpretation of the zoning in clinopyroxene reflected in Fig. 2, gives a temperature of the order of 750 °C. Whereas this thermometry is complicated by the retrograde reaction, as well as by the uncertainties involved in the application of the thermometer, it seems clear that the metamorphic temperature at high pressure was less than 800 °C.

Trace element thermometry of zircon and rutile

Trace element thermometry is uniquely suitable for recording crystallization temperatures of accessory phases (Watson *et al*., 2006), for example using the increasing solubility of Ti in zircon or Zr in rutile with increasing temperature (Watson & Harrison, 2005). The closure temperature for the Ti-in-zircon thermometer is likely to be exceptionally high as other 4^+ cations (Hf, Th, U) are effectively immobile at all plausible geological conditions (Watson *et al*., 2006). In contrast, rutile is moderately retentive of Zr chemical signatures, with diffusivities within an order of magnitude of those for Pb in rutile over most geological conditions (Cherniak *et al*., 2007).

These thermometers have been applied to zircon and rutile from the Southern domain eclogite, sample 01SZ40b, that was also dated by both ID-TIMS and SHRIMP analysis (Baldwin *et al*., 2004). This sample contains the complete buffering assemblage of zircon, rutile and quartz. ID-TIMS analysis of zircon in this sample records a mixing line between 2.54 and 1.9 Ga. Zircon inclusions in clinopyroxene from the same sample were analysed by SHRIMP and yield a single population of *c*. 1.9 Ga dates (Baldwin *et al*., 2004). Single grain analyses of rutile from the same sample yielded $^{207}Pb/^{206}Pb$ dates of 1882–1851 Ma (Baldwin *et al*., 2004).

Analysis for zircon thermometry was made by LA-ICP-MS on the Finnigan Element 2 ICP-MS equipped with a Nd:YAG UP-213-nm laser ablator at the University of Maryland. Analysis of the lesser isotope of titanium, Ti-49, is necessary because of the isobaric interference of Zr-96 with Ti-48. A spot size of 25 μm was used and results were normalized against Hf concentrations, which were measured by electron microprobe analysis.

Ten spot analyses from the zircon shown in Fig. 11a of Baldwin *et al*. (2004) were obtained with Ti concentrations ranging from 6 to 10 p.p.m., yielding a crystallization temperature of 720 ± 30 °C (2σ) using the revised calibration of Ferry & Watson (2007) (Table 1), assuming no pressure dependence of the thermometer. No significant intragrain variation was observed, nor were significant differences observed in rim *v*. core domains apparent in a CL image.

Zirconium analysis of rutile was performed on the Cameca Ultrachron electron microprobe at the University of Massachusetts. The analysis was made via trace-element mode, using a theoretical TiO_2 composition for the matrix and measuring only Zr. This measurement was performed by integrating Zr counts (using the ZrLα line) from five spectrometers using a focused 20 kV beam at 200 nA. The following monochromators were used: PET, two Large PETs and two Very Large PETs (with accompanying VL detectors). Sample backgrounds were obtained by detailed WDS scanning in the ZrLα wavelength region and extracting the background intensity by regression of scan data by polynomial regression. Natural zircon was used for calibration. Peak count time on the unknown was

Table 1. LA-ICP-MS analyses of Ti, REE and Y in eclogite zircon (concentrations in p.p.m.).

Label	Ti	Y	La	Ce	Pr	Nd	Sm	Eu	Gd	Tb	Dy	Ho	Er	Tm	Yb	Lu
01SZ40b-1	7	85	< 0.41	9	< 0.32	1.0	< 1.27	0.5	< 2.86	0.7	8	2.8	13	2.8	27	5.5
01SZ40b-2	6	248	< 0.80	10	< 0.14	1.1	1.2	0.5	6.0	2.1	24	9.0	40	8.7	77	14.3
01SZ40b-3	10	135	< 0.32	12	0.1	< 1.51	1.4	< 1.25	3.4	1.2	13	4.6	22	4.5	40	7.4
01SZ40b-4	8	242	< 0.35	13	0.1	1.5	1.5	< 0.70	< 3.98	1.7	22	8.4	39	7.5	71	13.4
01SZ40b-5	7	22	0.5	7	0.5	3.9	2.1	< 0.60	< 4.77	0.5	3	0.7	2	< 0.65	3	< 0.77
01SZ40b-6	9	55	0.8	12	0.8	4.9	2.1	< 0.85	3.5	0.6	5	2.0	9	1.8	19	3.5
01SZ40b-7	10	83	1.6	15	1.2	7.8	2.4	< 0.74	3.2	0.7	8	2.7	12	3.1	26	5.2
01SZ40b-8	7	242	< 0.37	11	< 0.14	1.3	< 4.52	< 0.71	5.8	2.0	23	8.9	39	7.9	73	14.8
01SZ40b-9	6	19	2.0	16	1.9	14.2	3.5	1.1	< 2.57	0.3	2	0.6	2	0.5	3	0.7
01SZ40b-10	8	334	< 0.28	7	< 0.21	1.3	< 3.90	0.3	9.3	2.6	32	11.7	52	10.2	99	18.4

Table 2. Zr concentration in rutile from eclogite (electron microprobe analyses).

Sample	Label	Analyses (*n*)	Zr (p.p.m.)	3 × SD (p.p.m.)	Petrographic setting	*T* (°C)[a]	*T* (°C)[b]
01SZ40b	Rutile-1	15	913	5	Inclusion in grt	743	777
01SZ40b	Rutile-2	10	1193	6	Inclusion in grt	770	805
01SZ40b	Rutile-3	15	1235	8	Inclusion in grt	774	809

[a]Ferry & Watson (2007); [b]Tomkins *et al.* (2007) calculated at $P = 16$ kbar.

600 s per point. Three rutile grains were analysed, obtaining 15 points for rutile 1, 10 points for rutile 2 and 15 points for rutile 3. The above conditions result in a single point detection limit of 14 p.p.m. (3σ) for Zr. The grain average yields an overall detection limit of 3 p.p.m. (3σ) for 15 points and 4 p.p.m. (3σ) for 10 points.

Rutile occurs exclusively as inclusions in garnet in 01SZ40b. Zr concentrations ranged from 913 to 1235 p.p.m. (Table 2). Forty analyses of three rutile inclusions yielded a crystallization temperature of 762 ± 34 °C (2σ) using the revised calibration of Ferry & Watson (2007) and 797 ± 34 °C (2σ) at 16 kbar (see below) using the new pressure-dependent calibration of Tomkins *et al.* (2007). The zircon and rutile results together with the garnet–clinopyroxene results described above imply that maximum temperatures during 1.9 Ga high-*P* metamorphism were ~ 750 °C, and were at least 250 ° lower than would be required to form ternary feldspar in the felsic gneisses.

Calculated pseudosections

In order to constrain the maximum pressures, as well as the *P–T* path, the observed mineral assemblages and compositions are compared with the stability and compositions of phases in *P–T–X* pseudosections. First, the amount of H_2O present in the protolith is constrained using *P–M*(H_2O) pseudosections, where *M*(H_2O) is the mol.% H_2O in the bulk composition. This composition is then used to calculate a *P–T* pseudosection to investigate the peak conditions and retrograde evolution of the eclogite.

The pseudosection modelling was made using THERMOCALC v. 3.25 (Powell *et al.*, 1998; recent upgrade) and the internally consistent thermodynamic data set 5.5 (Holland & Powell, 1998; November 2003 upgrade) in the system Na_2O–CaO–FeO–MgO–Al_2O_3–SiO_2–H_2O (NCFMASH). The activity–composition relationships of the minerals used in the calculations follow the orthopyroxene model of White *et al.* (2001), the clinopyroxene model of Holland & Powell (1996), the plagioclase model of Holland & Powell (2003) and the amphibole model of Dale *et al.* (2005). The highest-*T* portions of the pseudosections are metastable with respect to melt-bearing assemblages, in the absence of a melt model for mafic bulk compositions.

The bulk composition of the sample used for the pseudosection analysis corresponds to sample 01SZ41a of Baldwin *et al.* (2004) determined by XRF analysis (in wt%): $SiO_2 = 42.75$, $Al_2O_3 = 20.37$, $Fe_2O_3 = 9.58$, $MnO = 0.13$, $MgO = 14.86$, $CaO = 10.29$, $Na_2O = 1.05$, $K_2O = 0.45$, $TiO_2 = 0.16$, $P_2O_5 = 0.03$. The peak mineral assemblage described in Baldwin *et al.* (2004) is garnet, clinopyroxene, kyanite, rutile, zoisite and quartz. Pargasitic amphibole occurs as large matrix grains as well as kelyphitic rims around garnet, possibly representing stability throughout the eclogite evolution. Retrograde phases include plagioclase, orthopyroxene, secondary clinopyroxene, phlogopite, spinel and sapphirine. Mineral compositions and zoning are described in Baldwin *et al.* (2004).

In order to estimate the amount of H_2O present in the bulk as well as to constrain peak pressure conditions, a *P–M*(H_2O) pseudosection was constructed for 750 °C (Fig. 3). This diagram contoured for X_{Jd} constrains peak pressures to ~16 kbar, based on the maximum observed X_{Jd} values in the Southern domain eclogite of ~0.25 (Fig. 3a). Notably, clinopyroxene is not present at H_2O-saturated conditions for this pressure, and only exists at higher pressure for much higher values of X_{Jd} than are observed in the rocks. This places the rocks at peak within the H_2O-undersaturated field of garnet–clinopyroxene–amphibole–zoisite–kyanite–quartz just above the stability of plagioclase (Fig. 3b). Kyanite and zoisite are observed in the eclogites, but generally occur as inclusions in garnet, which are interpreted to be the products of plagioclase breakdown along the prograde path. The apparent stability of kyanite and zoisite at peak conditions may be related to the relatively high Ca-Tschermak's content of the clinopyroxene ($X_{CaTs} = 0.10$), which the activity–composition model does not incorporate. Alternatively, as the predicted modes of kyanite and zoisite present at peak are relatively small (8 and 4 mol.% respectively), it is likely they would not survive decompression and the extensive symplectite overprinting that has affected the rocks. Importantly, the pseudosection predicts the stability of amphibole at peak conditions. To place constraints on the amount of H_2O that may have been present in the bulk, a value was chosen that corresponds to the approximate mode of primary amphibole present in the rocks, which is estimated at ~10%. This corresponds to an *M*(H_2O) value of ~ 1 mol.%. The composition of amphibole in the eclogite is pargasitic with compositions of a(hb) [X_{Na}, A] = 0.55–0.65 and z(hb) [X_{Na}, M4] = 0.10, indicating equilibration at pressures of 12–14 kbar (Fig. 3c,d). This *M*(H_2O) corresponds to a fluid with $a(H_2O)$ of ~0.2. Large primary grains have a similar composition to kelyphites surrounding garnet, and are inferred to have formed at higher pressures but later re-equilibrated following decompression.

A *P–T* pseudosection was constructed for a bulk composition with 1 mol.% H_2O to investigate the *P–T* stability of other retrograde phases, including plagioclase and orthopyroxene (Fig. 4). This diagram is

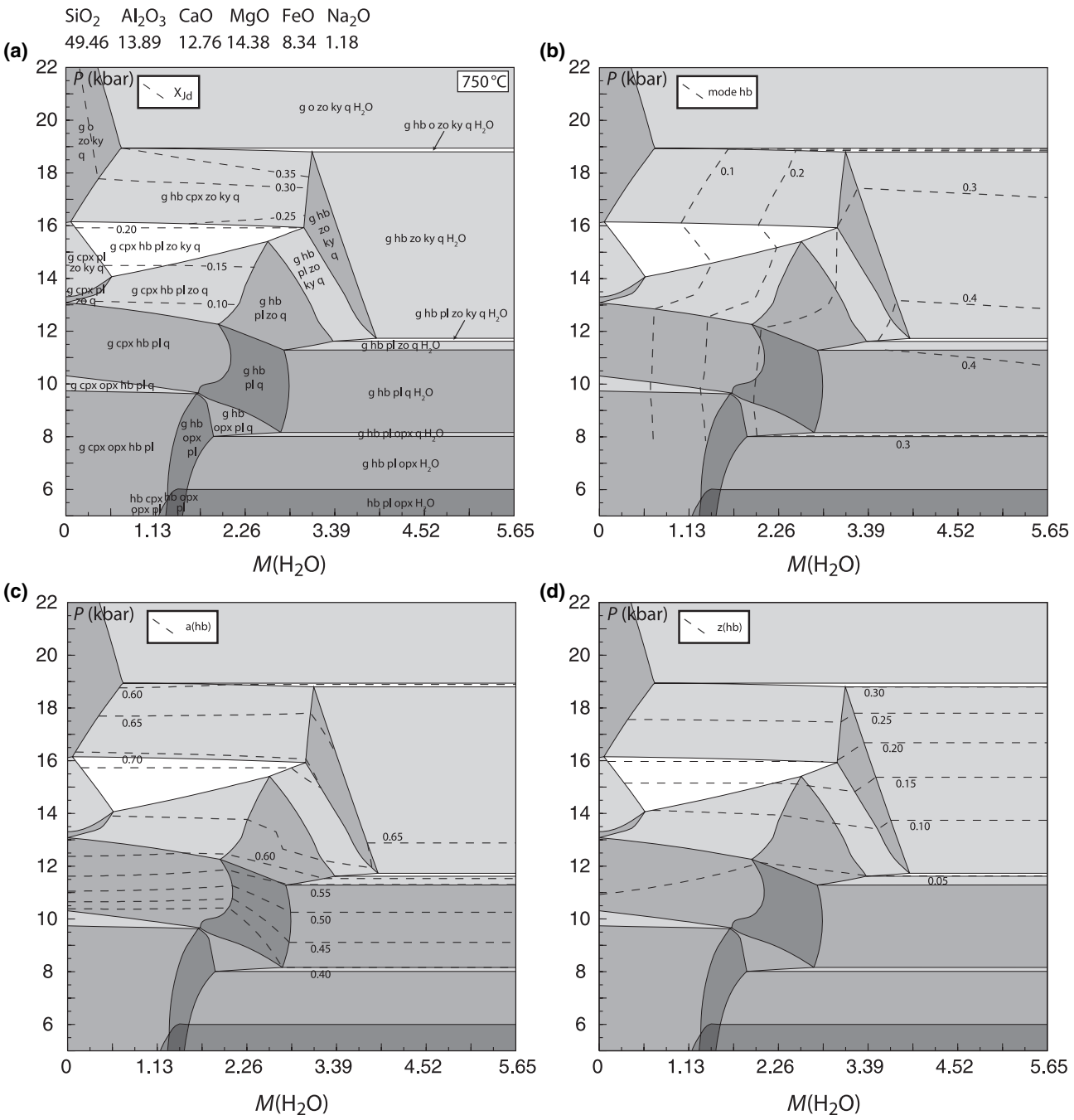

Fig. 3. Pressure *v.* $M(H_2O)$ pseudosections for eclogite bulk composition calculated at 750 °C with $M(H_2O)$ ranging from 0 to 5.65 mol.%. Bulk composition is given in mol.%. cpx, clinopyroxene; g, garnet; hb, hornblende; ky, kyanite; o, omphacite; opx, orthopyroxene; pl, plagioclase; q, quartz; zo, zoisite. (a) Contoured for X_{Jd} (dashed lines); (b) contoured for mol.% of hornblende; (c) contoured for a(hb) = [X_{Na}, A]; (d) contoured for z(hb) = [X_{Na}, M4].

contoured for both X_{Jd} and X_{An}. At peak conditions corresponding to 16 kbar and 750 °C, the composition of clinopyroxene is consistent with the observed mineral composition. Plagioclase is not stable at peak conditions, but becomes stable immediately upon decompression, with a composition of $X_{An} = 0.25$–0.30, which is also consistent with the observed mineral compositions, although the comparison is made difficult by the fact that the eclogite had become domainal in composition by this stage. Orthopyroxene stability is limited to ≤10 kbar. This implies that amphibole began forming at higher pressure along the retrograde path, followed by orthopyroxene after substantial decompression. The relatively low pressure stabilization of

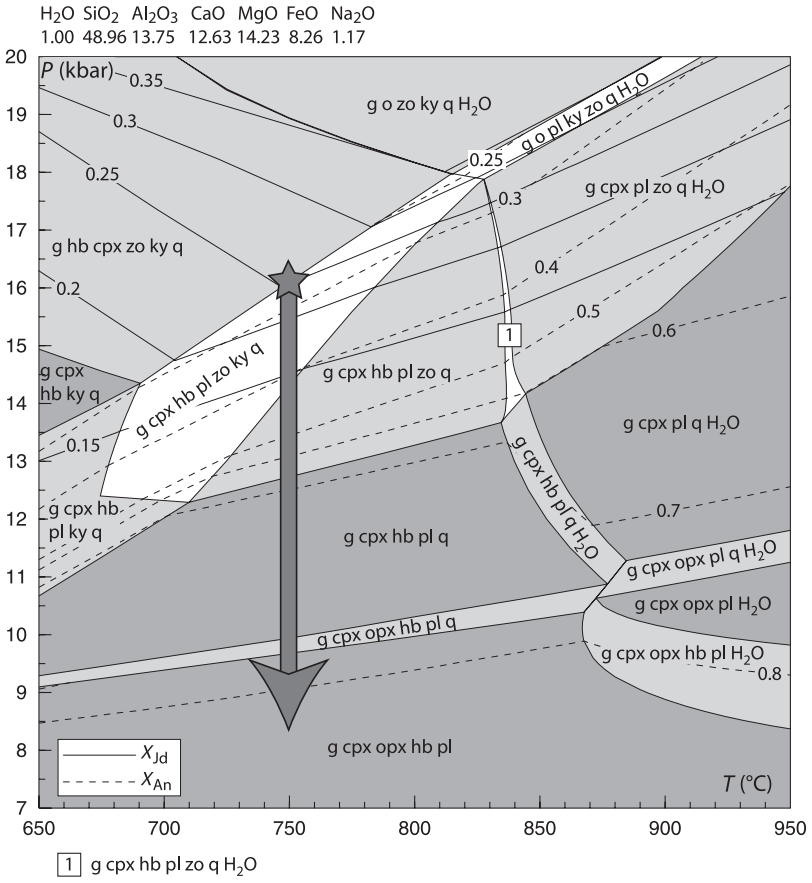

Fig. 4. *P–T* pseudosection for eclogite with 1 mol.% H_2O in bulk composition. Star indicates peak metamorphic conditions at 16 kbar, 750 °C. Arrow shows isothermal decompression path at 750 °C. Contours are shown for X_{Jd} (solid lines) and X_{An} (dashed lines).

orthopyroxene is relevant for understanding the development of the layered structure that occurs along kyanite veins in the eclogite, as considered below. These observations are consistent with a decompression path at 750 °C from 16 kbar down to at least 10 kbar.

Importantly, this analysis demonstrates that the decompression history of the eclogite is consistent with the rocks having little H_2O added during retrogression. In fact it is conceivable that the complete evolution of the eclogite occurred at nearly constant H_2O content, not having been H_2O-saturated at any stage. If the original rock was H_2O-saturated it must have become H_2O-undersaturated prior to the peak of metamorphism. The final stage of decompression can be constrained by the presence of sapphirine–plagioclase and spinel–plagioclase symplectites after kyanite that are described below.

Fig. 5. Outcrop of sapphirine–kyanite-bearing veins within eclogite. Hammer is aligned with foliation. Veins are generally parallel to the main fabric, but also crosscut the fabric.

ORIGIN OF SAPPHIRINE- AND SPINEL-BEARING ROCKS

Sapphirine- and spinel-bearing rocks occur in association with eclogite in the Southern domain (Snoeyenbos *et al.*, 1995; Baldwin *et al.*, 2004). Such rocks occur in two contexts. The first is as a narrow (1–2 m) zone between the eclogite and the felsic gneiss. The second is in centimetre-scale, originally kyanite-bearing, veins within the eclogite (Fig. 5). Both contexts involve the replacement of kyanite by sapphirine–plagioclase and spinel–plagioclase symplectites, with the degree of breakdown of the kyanite being variable.

Lithologies, textures and mineral compositions are described below, with an emphasis on assemblages and textures relevant to petrological modelling. In order to

Table 3. Representative garnet compositions from sapphirine-bearing rocks (electron microprobe analyses).

Sample	01SZ40A	01SZ40A	01SZ133C	01SZ133C	01SZ133C	01SZ133C	01SZ133C	01SZ100E	01SZ100E
Type	core	rim	core	near pl incl	rim nr pl	rim nr opx	rim nr plag	adj pl	adj opx
SiO_2	39.78	38.89	39.76	39.39	39.07	39.58	39.51	39.37	39.68
TiO_2	0.05	0.04	0.09	0.02	0.06	0.03	0.07	0.02	0.05
Al_2O_3	22.91	22.61	23.03	23.11	22.44	22.83	22.37	23.10	22.78
Cr_2O_3	0.064	0.077	0.02	bd	bd	bd	0.02	bd	bd
FeO	20.11	23.26	17.10	22.71	23.62	23.16	22.43	22.74	17.04
MnO	0.18	0.22	0.33	0.51	0.61	0.58	0.51	0.74	0.32
MgO	10.65	8.19	7.91	9.24	9.57	10.85	9.93	10.92	9.46
CaO	6.38	6.62	12.38	5.51	4.77	3.37	5.89	2.90	10.15
Na_2O	0.06	0.01	bd	bd	bd	bd	0.01	bd	bd
Total	100.17	99.92	100.63	100.48	100.15	100.41	100.73	99.78	99.47
Si	2.98	2.97	2.98	2.98	2.98	2.98	2.98	2.98	2.99
Ti	0.00	0.00	0.01	0.00	0.00	0.00	0.00	0.00	0.00
Al	2.03	2.04	2.04	2.06	2.01	2.03	1.99	2.06	2.02
Cr	0.00	0.00	0.00	0.00	0.00	0.00	0.00	0.00	0.00
Fe^{2+}	1.26	1.49	1.07	1.44	1.50	1.46	1.42	1.44	1.07
Mn	0.01	0.01	0.02	0.03	0.04	0.04	0.03	0.05	0.02
Mg	1.19	0.93	0.88	1.04	1.09	1.22	1.12	1.23	1.06
Ca	0.51	0.54	0.99	0.45	0.39	0.27	0.48	0.23	0.82
Na	0.01	0.00	0.00	0.00	0.00	0.00	0.00	0.00	0.00
X_{Grs}	0.17	0.18	0.33	0.15	0.13	0.09	0.16	0.08	0.28
X_{Sps}	0.00	0.00	0.01	0.01	0.01	0.01	0.01	0.02	0.01
X_{Alm}	0.42	0.50	0.36	0.49	0.50	0.49	0.47	0.49	0.36
X_{Prp}	0.40	0.31	0.30	0.35	0.36	0.41	0.37	0.42	0.36

Normalized to 12 oxygen. bd, below detection limit.

evaluate compositional zonation, high-resolution compositional maps of these assemblages were collected on the Cameca SX-50 microprobe at the University of Massachusetts. Mineral compositions were measured on the JEOL Superprobe 733 at MIT using an accelerating voltage of 15 kV and a beam current of 10 nA. Locations of spot analyses and quantitative traverses were selected based on the zonation and variation evident in high-resolution compositional maps. Representative mineral analyses are given in Tables 3–6.

Sapphirine-bearing marginal rocks

The rocks that occur at the margin of the eclogite unit contain the assemblage garnet + kyanite + quartz interpreted to be a primary high-pressure assemblage. Garnet shows strong Ca-depletion at the rim adjacent to surrounding plagioclase, and there is also a narrow zone of Fe–Mg exchange at the rim. The Ca content of garnet cores is variable, with compositions ranging in $Prp_{40-30}Alm_{42-36}Grs_{17-33}$ (Table 3). There are two microstructures associated with garnet. Garnet is either surrounded by a composite corona of plagioclase and orthopyroxene in the vicinity of quartz, or, where garnet is adjacent to kyanite, it is rimmed by sapphirine- or spinel-bearing symplectites. In the first setting, garnet is typically rimmed by a corona of plagioclase, which is, in turn, rimmed by orthopyroxene (Figs 6a & 7a,b). Garnet typically contains abundant inclusions of kyanite, quartz, and plagioclase (Fig. 7b). Orthopyroxene has X_{Mg} of 0.66–0.67 (Table 4). Plagioclase between garnet and orthopyroxene is relatively sodic with a composition of An_{43-48} (Table 5).

Kyanite occurs as either discrete or clustered 200–400 μm porphyroblasts (Figs 6b & 7c), replaced by sapphirine- and spinel-bearing symplectites. These form two discrete symplectite microstructures, with extremely fine-grained symplectites involving sapphirine–plagioclase directly adjacent to the kyanite, surrounded by a symplectite involving larger, discrete spinel grains embedded in plagioclase (Fig. 7c). The composition of the plagioclase in these symplectites is typically An_{77-79} (Table 5). Sapphirine is more magnesian than spinel in adjacent symplectites, with X_{Mg}

Table 4. Representative orthopyroxene compositions from sapphirine-bearing rocks (electron microprobe analyses).

Sample	01SZ40A	01SZ133C	01SZ133C	01SZ100E
Type	corona	corona	nr pl	core
SiO_2	52.37	52.96	52.30	54.73
TiO_2	0.05	0.07	0.09	0.04
Al_2O_3	3.16	2.26	4.62	1.50
Cr_2O_3	0.17	bd	0.17	0.02
FeO	21.10	20.49	18.00	16.83
MnO	0.04	0.14	0.14	0.20
MgO	23.21	23.87	25.22	26.73
CaO	0.12	0.16	0.17	0.41
Na_2O	0.01	bd	bd	bd
Total	100.24	99.95	100.71	100.46
Si	1.93	1.95	1.89	1.97
Ti	0.00	0.00	0.00	0.00
Al	0.14	0.10	0.20	0.06
Cr	0.00	0.00	0.00	0.00
Fe^{2+}	0.65	0.63	0.54	0.51
Mn	0.00	0.00	0.00	0.01
Mg	1.27	1.31	1.36	1.43
Ca	0.00	0.01	0.01	0.02
Na	0.00	0.00	0.00	0.00
X_{Mg}	0.66	0.67	0.71	0.74

Normalized to 6 oxygen. bd, below detection limit. $X_{Mg} = Mg/(Mg + Fe^{2+})$.

Table 5. Representative plagioclase compositions from sapphirine-bearing rocks (electron microprobe analyses).

Sample	01SZ40A	01SZ40A	01SZ40A	01SZ40A	01SZ40A	01SZ133C	01SZ133C	01SZ133C	01SZ133C	01SZ133C	01SZ133C	01SZ100E	01SZ100E	01SZ100E
Type	corona	matrix	adj spl	adj spl	adj spr	incl in grt	Corona	nr qtz	nr spr	adj ky	crn sym	adj spr	adj spl	nr grt
SiO_2	55.57	56.90	48.79	53.87	48.65	57.86	57.55	59.88	44.63	44.99	44.17	46.31	46.71	49.50
Al_2O_3	28.42	27.95	33.75	30.16	33.58	26.50	27.26	25.61	35.64	35.49	36.39	35.12	35.16	32.74
FeO	0.24	0.15	0.22	0.27	0.32	0.19	0.25	bd	0.15	0.09	0.02	0.09	0.16	0.27
MgO	0.02	0.02	0.12	0.05	0.20	bd	bd	bd	bd	0.01	bd	0.01	bd	bd
CaO	9.84	9.58	15.52	11.79	15.82	8.32	9.10	6.94	18.82	18.51	18.52	17.58	18.00	15.35
Na_2O	5.81	6.15	2.56	4.84	2.32	6.75	6.52	7.50	0.78	0.93	0.73	1.40	1.40	2.84
K_2O	0.10	0.19	0.06	0.13	0.06	0.09	0.09	0.17	0.02	0.02	0.02	bd	0.01	0.02
Total	99.99	100.95	101.02	101.11	100.96	99.71	100.77	100.10	100.03	100.04	99.85	100.51	101.44	100.72
Si	2.50	2.53	2.21	2.41	2.21	2.60	2.56	2.66	2.06	2.07	2.04	2.12	2.12	2.25
Al	1.51	1.47	1.80	1.59	1.79	1.40	1.43	1.34	1.94	1.93	1.98	1.89	1.88	1.75
Fe^{2+}	0.01	0.01	0.01	0.01	0.01	0.01	0.01	0.00	0.01	0.00	0.00	0.00	0.01	0.01
Mg	0.00	0.00	0.01	0.00	0.01	0.00	0.00	0.00	0.00	0.00	0.00	0.00	0.00	0.00
Ca	0.47	0.46	0.75	0.57	0.77	0.40	0.43	0.33	0.93	0.91	0.92	0.86	0.87	0.75
Na	0.51	0.53	0.22	0.42	0.20	0.59	0.56	0.65	0.07	0.08	0.07	0.12	0.12	0.25
K	0.01	0.01	0.00	0.01	0.00	0.00	0.00	0.01	0.00	0.00	0.00	0.00	0.00	0.00
X_{An}	0.48	0.46	0.77	0.57	0.79	0.40	0.43	0.34	0.93	0.92	0.93	0.87	0.88	0.75

Normalized to 8 oxygen. bd, below detection limit.

Table 6. Representative sapphirine and spinel compositions from sapphirine-bearing rocks (electron microprobe analyses).

Sample	01SZ40A	01SZ40A	01SZ133C	01SZ133C	01SZ100E	01SZ100E
Mineral	spr	spl	spr	Spl	Spr	spl
SiO_2	12.06	0.05	11.54	0.02	11.59	0.01
TiO_2	0.02	0.01	0.01	0.01	bd	bd
Al_2O_3	62.68	62.55	64.25	61.71	64.40	61.90
Cr_2O_3	0.18	0.69	bd	0.01	bd	bd
FeO	8.69	24.09	8.86	26.73	9.05	26.28
MnO	bd	0.02	0.07	0.10	0.08	0.09
MgO	15.49	11.68	14.91	10.84	14.91	11.44
CaO	0.02	0.05	0.01	0.07	bd	0.05
NiO	bd	0.45	bd	0.13	bd	0.06
Total	99.13	99.59	99.65	99.62	100.03	99.84
Si	0.72	0.00	0.69	0.00	0.69	0.00
Ti	0.00	0.00	0.00	0.00	0.00	0.00
Al	4.44	1.97	4.53	1.96	4.53	1.95
Cr	0.01	0.01	0.00	0.00	0.00	0.00
Fe^{3+}	0.10	0.01	0.09	0.04	0.09	0.05
Fe^{2+}	0.34	0.52	0.36	0.56	0.36	0.54
Mn	0.00	0.00	0.00	0.00	0.00	0.00
Mg	1.39	0.47	1.33	0.43	1.33	0.46
Ca	0.00	0.00	0.00	0.00	0.00	0.00
Ni	0.00	0.01	0.00	0.00	0.00	0.00
X_{Mg}	0.80	0.47	0.79	0.44	0.79	0.46

Sapphirine normalized to 10 and spinel to 4 oxygen. Ferric iron calculated by charge balance. bd, below detection. $X_{Mg} = Mg/(Mg + Fe^{2+})$.

of 0.79–0.80 and 0.44–0.47 respectively (Table 6). Kyanite can be found in direct contact with garnet, but more commonly symplectites of sapphirine–plagioclase and spinel–plagioclase occur directly adjacent to garnet and are inferred to be former kyanite grains that have been completely pseudomorphed by these symplectites (Fig. 7d). In addition, clusters of corundum + anorthite are less commonly observed, which may represent former sites of kyanite porphyroblasts that have been completely pseudomorphed.

Quartz is never observed to be in contact with sapphirine- or spinel-bearing microstructures, always being separated from them by a moat of plagioclase. In contrast, quartz abuts the garnet microstructures, with a thin selvage of orthopyroxene between quartz and plagioclase (Fig. 7a). The composition of plagioclase in the garnet coronas is more sodic than in the kyanite-bearing sub-domains (An_{57}) (Table 5).

Accessory minerals include rutile, ilmenite, zircon and apatite. Rutile is abundant and occurs both in association with the sapphirine symplectites and as inclusions in garnet. Apatite in one sample contains abundant needle-shaped inclusions and lamellae of monazite. Monazite has not been observed as a discrete phase in these rocks.

Quartz-absent sapphirine-bearing veins

Quartz-undersaturated sapphirine-bearing symplectites after kyanite occur as veins within the eclogite unit (Fig. 5). These veins are typically a few centimetre wide and generally are concordant with the main

Fig. 6. Photomicrographs from sapphirine granulites. (a) Garnet with orthopyroxene–plagioclase corona surrounded by matrix quartz. (b) Kyanite surrounded by symplectites of sapphirine–plagioclase and spinel–plagioclase. Plagioclase moat around reaction texture separates symplectites from quartz. (c) Kyanite vein with symplectite development along margin producing sapphirine–spinel–corundum symplectites with plagioclase. Plagioclase layer occurs below. Adjacent to this is an orthopyroxene–plagioclase symplectite. (d) Vein texture showing spinel–plagioclase symplectite immediately adjacent to kyanite which is rimmed by the sapphirine–plagioclase symplectite. Corundum–plagioclase symplectites overgrew these symplectites. (e) Resorbed, elongate garnet porphyroblast adjacent to plagioclase layer below vein. Garnet is directly adjacent to plagioclase on the vein side of the texture, but below, closer to the orthopyroxene layer, development of extensive symplectites of orthopyroxene–plagioclase is visible. Same garnet for which compositional traverse is shown in Fig. 9. (f) Orthopyroxene porphyroblast within vein structure. Large (1–5 mm) orthopyroxene porphyroblasts are commonly interlayered with kyanite veins. These typically show extensive reaction to symplectites consisting of orthopyroxene–clinopyroxene–hornblende–plagioclase. Sapphirine is visible in the upper right-hand corner of the field of view.

foliation. In some locations, the veins form a more extensive network that crosscuts the foliation at a large angle (Fig. 5). In some outcrops these veins are closely spaced, and form a zone, no more than 10 cm wide, that consists of monomineralic kyanite, plagioclase, garnet and orthopyroxene layers (Fig. 8). In these zones, garnet is slightly more Fe-rich and less Mg-rich in the vein compared with garnet in the eclogite

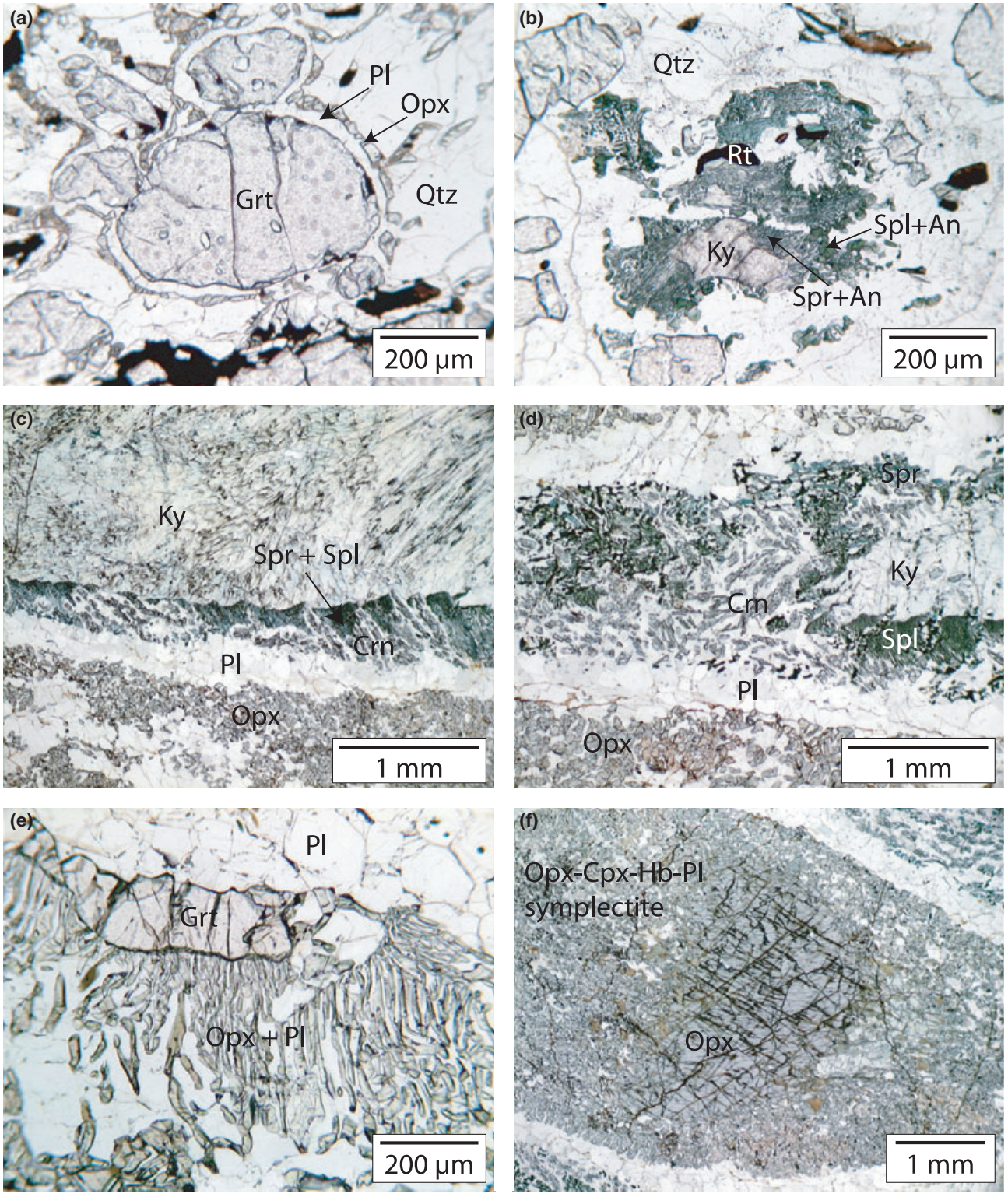

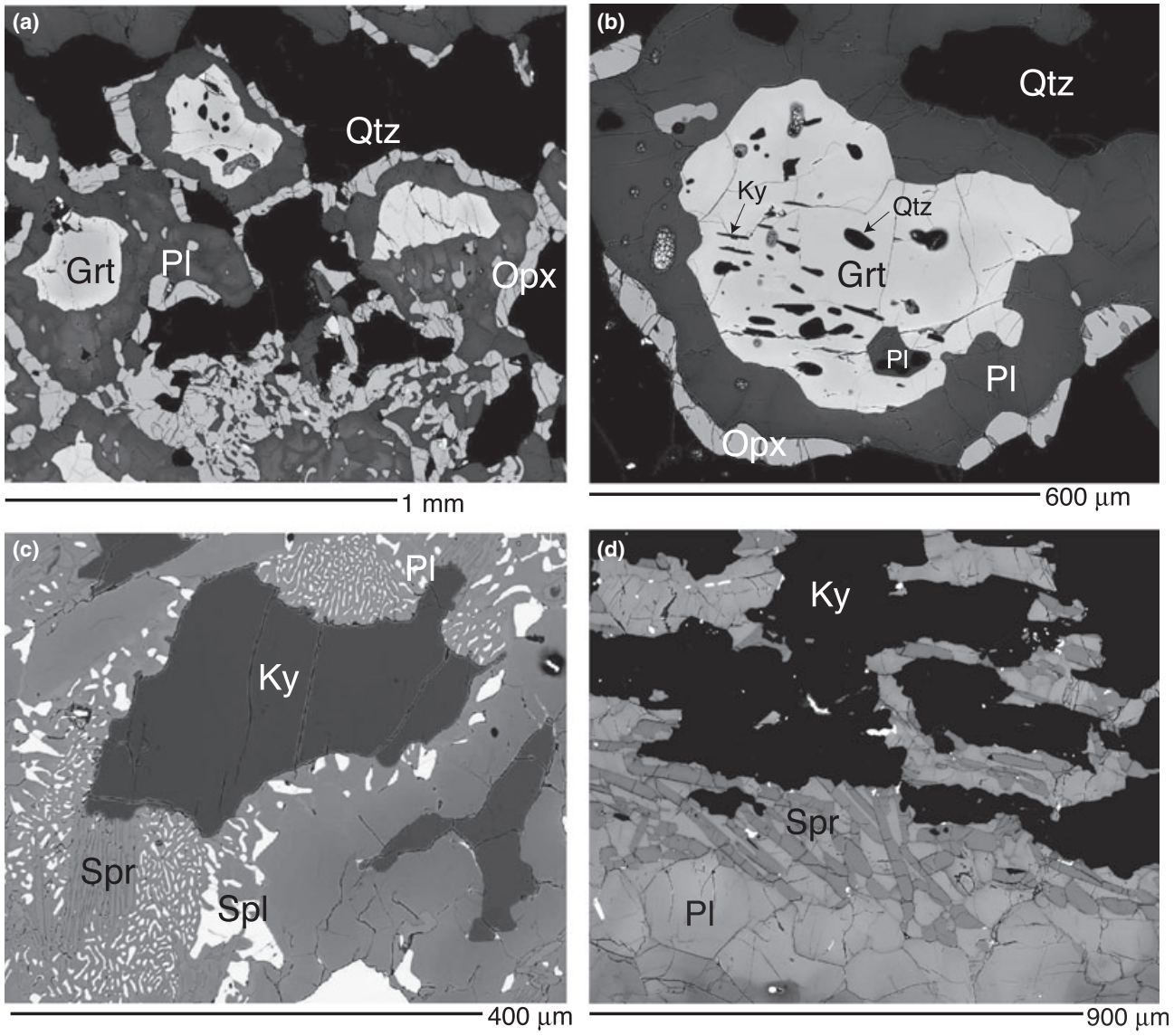

Fig. 7. Backscattered electron images. (a) Corona texture in Qtz-bearing sapphirine rocks. Corona of plagioclase surrounds garnet, which is surrounded by a thin layer of orthopyroxene. Quartz is present on the outside of corona microstructure. (b) Similar corona textures around garnet as in (a). Garnet contains inclusions of kyanite, plagioclase and quartz. (c) Kyanite porphyroblast surrounded by symplectites of Spr–Pl and Spl–Pl. Entire grain is surrounded by moat of plagioclase, which separates it from matrix quartz. (d) Kyanite vein with Spr–Pl symplectite at margin.

($Alm_{36}Prp_{36}Grs_{28}$ in vein compared with Alm_{33-23} $Prp_{43-55}Grs_{17-29}$ in the eclogite) (Table 3).

The kyanite veins are replaced by fine-grained symplectites of spinel–plagioclase and sapphirine–plagioclase, with a tendency for the sapphirine-bearing symplectite to occur adjacent to the kyanite and the spinel-bearing symplectites to be away from the kyanite (Fig. 6c,d). Sapphirine–plagioclase symplectites may appear to overgrow spinel–plagioclase symplectite, and both symplectites appear to be overgrown by corundum–plagioclase symplectite (Fig. 6c,d). Plagioclase in these symplectites is near-end-member anorthite with a composition of 0.87–0.93. The most calcic compositions occur adjacent to corundum. Sapphirine is more magnesian than spinel with X_{Mg} of 0.79 and 0.46 respectively. Discrete crystals of sapphirine are generally aligned along vein margins (Figs 6c & 7d). Small inclusions (≤10 μm) of monazite and allanite are common as inclusions in kyanite.

The symplectites just described appear to replace the kyanite layer itself, with the edge of the original layer being sharp against a zone or layer of near-end-member anorthite within the kyanite vein (Fig. 6e). Where sufficiently well preserved, in the context of commonly intense symplectite development, the plagioclase layer is succeeded outwards by garnet then orthopyroxene

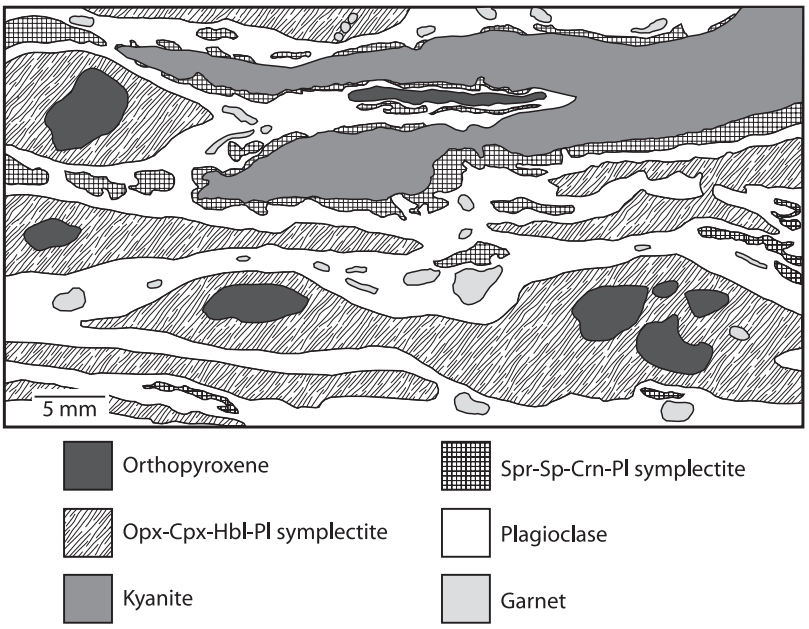

Fig. 8. Sketch of vein structure. Kyanite is interlayered with plagioclase, garnet and orthopyroxene forming a layered structure. These minerals react to form extensive symplectites. Spr–Spl–Crn–Pl symplectites occur adjacent to kyanite. Relict orthopyroxene porphyroblasts are preserved and are surrounded by complex symplectites, dominated by Opx–Pl, and lesser amounts of Cpx and Hbl. Smaller garnet porphyroblasts are distributed throughout the rock, and commonly are surrounded by Opx–Pl symplectites. Sketch is the size of a standard thin section.

layers (Fig. 6e). The garnet layer involves elongate and disrupted garnet porphyroblasts that are highly resorbed, due presumably to their participation in the symplectite-forming reactions replacing kyanite. Garnet typically shows highly asymmetric zoning profiles, with a strong depletion in Ca from Grs_{28} adjacent to the orthopyroxene to Grs_{12} adjacent to the vein (Fig. 9). A less dramatic increase in Fe and Mg is observed from $Alm_{38}Prp_{34}$ adjacent to orthopyroxene to $Alm_{49}Prp_{39}$ adjacent to the vein (Fig. 9). In the orthopyroxene layer, large orthopyroxene porphyroblasts are surrounded by symplectites of orthopyroxene–clinopyroxene–hornblende–plagioclase (Fig. 6f). These porphyroblasts have an X_{Mg} of 0.74 and are not very aluminous (1.5 wt% Al_2O_3). The asymmetric zoning seen in the garnet is consistent with the plagioclase–garnet–orthopyroxene layering away from the kyanite being a relatively large-scale corona structure. Accessory phases include monazite, allanite, rutile, ilmenite and zircon.

Orthopyroxene is also present in symplectites around large 1–5 mm garnet porphyroblasts. Also in the matrix, discrete spinel–plagioclase symplectites occur, with sapphirine–plagioclase symplectites. These microstructures are rimmed by a moat of near-end-member anorthite. These probably represent sites of former kyanite porphyroblasts.

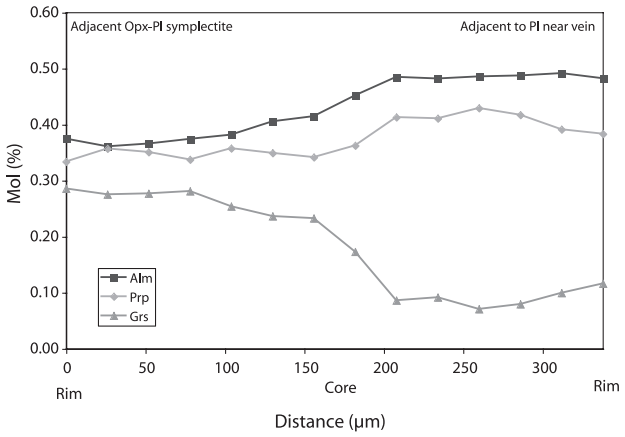

Fig. 9. Asymmetric garnet zoning profile in sapphirine granulite. Profile is shown for garnet in Fig. 6e. Left-hand side of the profile is adjacent to the Opx symplectite at the bottom of garnet. Right-hand side is adjacent to plagioclase that is adjacent to the Spr–Pl symplectites at the edge of the vein (off the field of view in Fig. 6e). Profile shows depletion in Grs on the side of garnet towards the vein as Ca is consumed to produce plagioclase. The Alm–Prp component in garnet is more depleted adjacent to Opx as Fe and Mg are consumed to produce Opx, and coexisting plagioclase in this symplectite is less anorthitic.

P–T MODELLING OF SAPPHIRINE- AND SPINEL-BEARING SYMPLECTITES

In order to place constraints on the development of these retrograde reaction textures, we undertook an approach of modelling the system using petrogenetic grids that consider variations in chemical potential of specific components in the system. This approach is necessary in rocks such as these where reaction textures develop involving one or more components entering into the site where the texture is developing, indicating open system behaviour. For example, in Fig. 7(c), kyanite surrounded by quartz is replaced by sapphirine–plagioclase and spinel–plagioclase, requiring at least CaO, FeO and MgO to be accessed by the kyanite from elsewhere in the rock for the reaction texture to be able to initiate and grow. Open system reaction textures cannot be investigated using a standard phase

diagram approach, with, for example, *P–T–X* pseudosections. The way to understand such textures is to investigate the phase equilibria using different thermodynamic variables (e.g. Powell *et al.*, 2005), in particular chemical potential rather than composition for more mobile components. Chemical potential has long been recognized as a critical control on mineral paragenesis and assemblage evolution (Korzhinskii, 1957); what distinguishes our approach is that it involves calculated phase equilibria. By examining such textures using this quantitative approach, the nature of these textures may be investigated.

In order to place *P–T* constraints on the development of sapphirine–plagioclase and spinel–plagioclase symplectites, an approach based on *P–T* petrogenetic grids for varying chemical potentials of the more mobile elements was used. The grids were calculated with THERMOCALC, using the same version and data set as used above. The system adopted was CFMAS, thus ignoring particularly Na_2O, for simplicity.

First, a petrogenetic grid for the full CFMAS system was constructed (Fig. 10). Here the general stability of the phases can be explored. In this grid, kyanite is metastable with respect to sillimanite. Each univariant reaction in this grid involves five phases, and thus contains more phases than are observed in symplectite-forming reactions, where typically only two or three phases are present. A method that effectively reduces the number of phases involved in each reaction is to fix the chemical potential of components, reducing the number of phases by one for each chemical potential that is fixed. For the CFMAS system, a new diagram was constructed by fixing the chemical potential of one of the mobile elements, in this case CaO (Fig. 11). The connection between Figs 10 and 11 is that along each univariant reaction in Fig. 10, the chemical potentials of each component continuously change. Therefore, a fixed value of μ_{CaO}, for example, will define an invariant point along each reaction as in Fig. 11. For example the g + sa = opx + sp + an + cor reaction in Fig. 10 becomes the invariant point to the right of the grey arrow in Fig. 11. These invariant points are then connected by new univariant reaction lines involving one less phase.

In order to evaluate how the variation in μ_{CaO} might affect the resulting symplectite development, it is necessary to examine how the topology of the reactions in Fig. 11 change as a function of μ_{CaO}. This is made with a P-μ_{CaO} diagram constructed at a fixed temperature of 750 °C (Fig. 12). This temperature was chosen as it lies directly down temperature of the cordierite-absent invariant point shown in Fig. 11, and it continues the isothermal decompression path in Fig. 10 down pressure. The path passes from where kyanite is stable at the onset of orthopyroxene growth in the kyanite veins at ~9–10 kbar, to the conditions of development of sapphirine–spinel–anorthite assemblages below ~7 kbar, below the univariant opx + cor = sa + sp + an where the necessary sapphirine–spinel–anorthite assemblage is stable (Fig. 11, shaded area). In

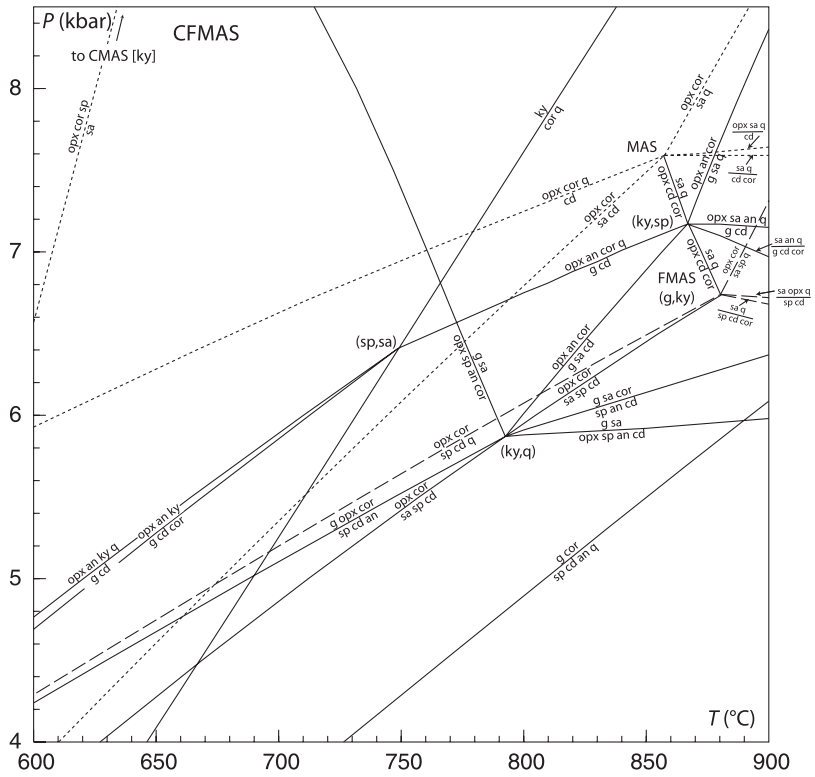

Fig. 10. CFMAS petrogenetic grid. With sillimanite excluded from consideration, reactions dominantly lie within corundum + quartz stability.

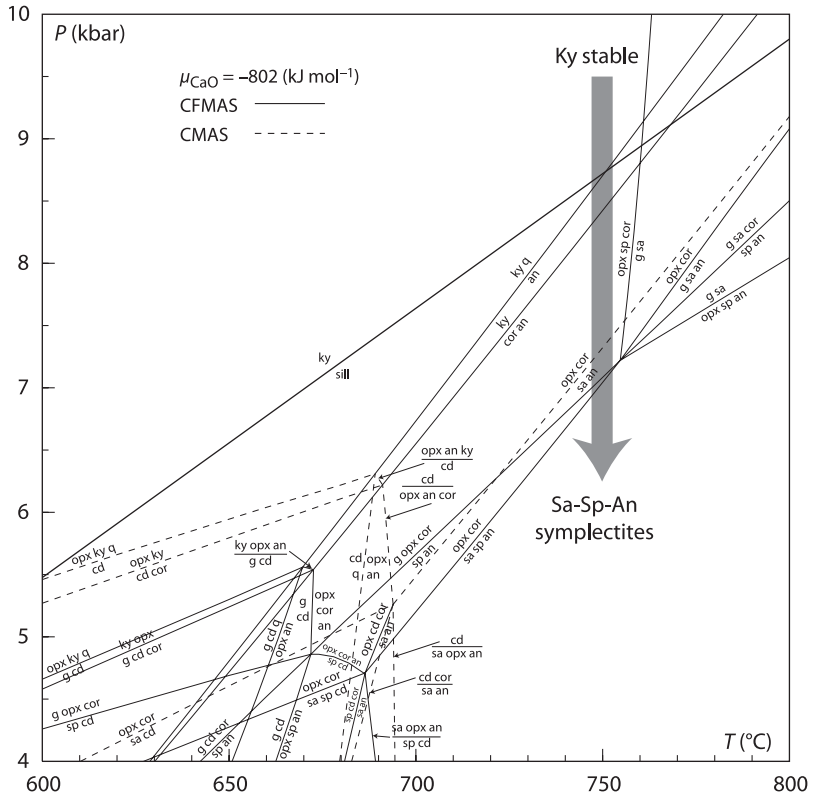

Fig. 11. CFMAS petrogenetic grid for fixed $\mu_{CaO} = -802$ (kJ mol^{-1}). Univariant reactions on Fig. 10 become invariant points on this diagram for the fixed value of μ_{CaO}. This results in univariant reactions with one less phase than Fig. 10. The kyanite vein assemblages develop at higher pressure within kyanite stability along the retrograde decompression path. Development of sa– sp–an symplectite assemblages is limited to ≤7.5 kbar for this value of μ_{CaO} along this path. The *P–T* path must occur to the left-hand side of this invariant, which limits the range of μ_{CaO} required for the development of these textures. Lower *P–T* stability is constrained by the absence of cordierite in these textures.

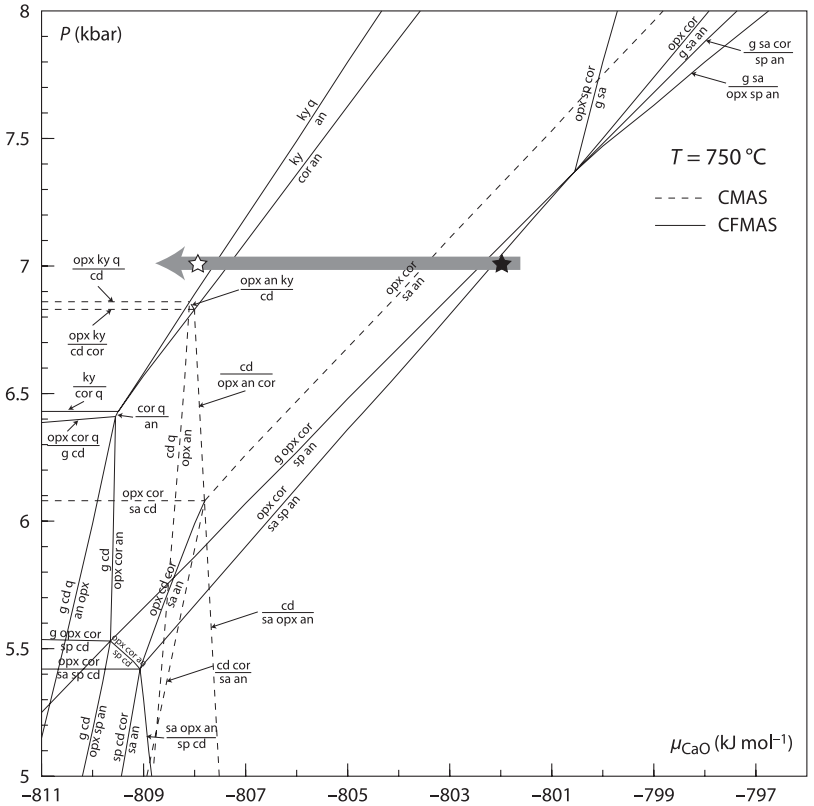

Fig. 12. *P*-μ_{CaO} diagram at fixed temperature (750 °C). The black star indicates μ_{CaO} for sa–sp–an assemblages at 7 kbar. The white star indicates μCaO for within kyanite. Arrow indicates decreasing μ_{CaO} between symplectites and the kyanite grains, indicating that a chemical potential gradient in CaO must be present between kyanite and the surrounding symplectites.

Fig. 12, it can be seen that adopting a static value of μ_{CaO} as was done in the construction of Fig. 11 is not useful in accounting for the reaction textures. If the symplectite development occurs at 7 kbar, the black star in Fig. 12 can be considered to correspond to μ_{CaO} at the kyanite edge where the symplectites are forming (where sa + sp + an is stable), whereas the white star corresponds to the kyanite itself (where kyanite is stable). The horizontal arrow represents the μ_{CaO} gradient that drives the replacement of kyanite by the symplectite. Figure 12 also shows that there is a relatively narrow pressure range that is consistent with the observed phase equilibria at 750 °C.

To explore the development of the two-phase symplectites (sa–an, sp–an and cor–an) it is necessary to consider the chemical potentials of two additional components, FeO and MgO. This can be explored by choosing a value of μ_{CaO} that corresponds to stable sapphirine–spinel–anorthite assemblages based on Fig. 12. Based on this analysis, a value of -802 kJ mol^{-1} was chosen for μ_{CaO}. At these conditions the sapphirine–spinel–anorthite assemblages will be produced at maximum pressures of 7 kbar.

A μ_{FeO}–μ_{MgO} diagram was then constructed for the fixed μ_{CaO} value defined above, corresponding to the black star shown on Fig. 12 (fixed P–T of 7 kbar and 750 °C) (Fig. 13). The three effectively invariant points on this diagram are g–sp–opx–an, opx–sp–sa–an and sp–sa–cor–an. Below the sp + an = sa reaction, sa + an is stable and above this reaction sp + an is stable. In order for sa + an and sp + an symplectite assemblages to develop, the topology of these three invariant points must be consistent with the arrangement shown in Fig. 13. Figure 14 shows the effect of changing P, T and μ_{CaO} on this topology. Figure 14(a) shows that an inversion of these invariants occurs at μ_{CaO} of around ~-805 kJ mol^{-1} at 7 kbar and 750 °C. Figure 14(b) limits pressure to $\sim$7 kbar at 750 °C and μ_{CaO} of -802 kJ mol^{-1}. Figure 14(c) limits temperature to $\sim$750 °C at $\sim$7 kbar and μ_{CaO} of -802 kJ mol^{-1}.

As Fig. 12 shows, the textures are developed under the action of a μ_{CaO} gradient, so that a μ–μ diagram such as Fig. 13 cannot account for all aspects of the textural development. The requisite would be a 3-D μ_{FeO}–μ_{MgO}–μ_{CaO} diagram. A qualitative representation of the μ path (representing the μ gradients) is shown in Fig. 15. This diagram accounts for the spatial development of the symplectite textures, with sapphirine–plagioclase adjacent to kyanite, and spinel–plagioclase developed distally. If it is considered that the μ_{CaO} gradient becomes progressively flattened with texture development, then sapphirine becomes progressively destabilized (grey arrows in Fig. 15), with corundum–anorthite symplectite developing. Finally, when the kyanite is consumed it leaves behind a patch of corundum + plagioclase symplectite.

The μ_{FeO}–μ_{MgO} diagram shown in Fig. 13 is contoured for spinel and sapphirine compositions and can be compared to the mineral chemistries of these min-

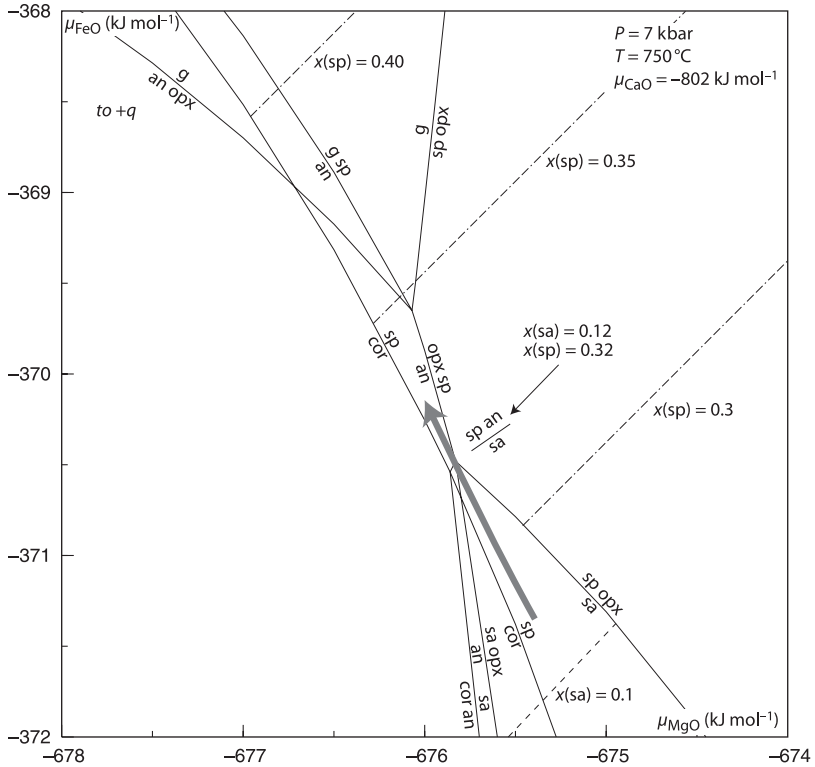

Fig. 13. μ_{FeO} *v.* μ_{MgO} diagram at fixed P, T and μ_{CaO}. Dash and dash-dot lines indicate contours for X_{Fe} in sapphirine and spinel respectively. Composition of sapphirine and spinel are also indicated at the sa = sp + an reaction. Grey arrow indicates the chemical potential path for generating first sa + an followed by sp + an assemblages.

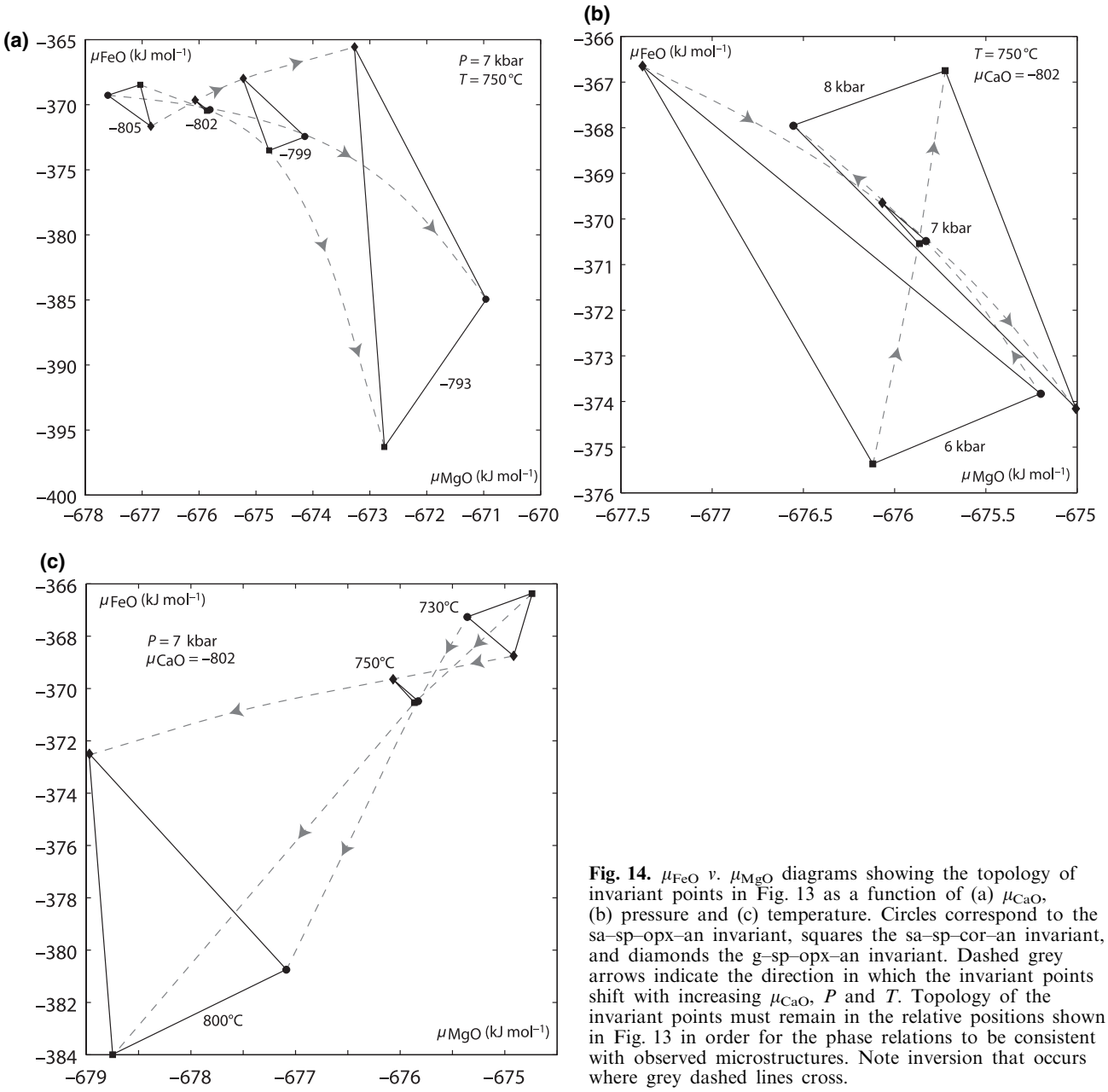

Fig. 14. μ_{FeO} *v.* μ_{MgO} diagrams showing the topology of invariant points in Fig. 13 as a function of (a) μ_{CaO}, (b) pressure and (c) temperature. Circles correspond to the sa–sp–opx–an invariant, squares the sa–sp–cor–an invariant, and diamonds the g–sp–opx–an invariant. Dashed grey arrows indicate the direction in which the invariant points shift with increasing μ_{CaO}, P and T. Topology of the invariant points must remain in the relative positions shown in Fig. 13 in order for the phase relations to be consistent with observed microstructures. Note inversion that occurs where grey dashed lines cross.

erals shown in Table 5. The composition of these phases right at the reaction sp + an = sa is X_{Fe} (sa) = 0.12 and X_{Fe} (sp) = 0.32 compared with ~0.2 and 0.5 for the observed compositions respectively. The predicted compositions are thus somewhat more Mg-rich than the observed compositions. Reasons for this include neglecting Na in the modelling and not adopting the precise *P–T* of development of the textures.

In summary, this chemical potential approach demonstrates the usefulness of fixed chemical potential grids and μ–μ diagrams for exploring the retrograde history of granulite facies terranes. In particular, this analysis demonstrates that the development of the symplectites and stability of sapphirine–spinel–anorthite assemblages is limited to ~ 750 °C and ≤7 kbar, and so corresponds to equilibration at uppermost amphibolite facies conditions.

DISCUSSION

P–T evolution of eclogite and associated sapphirine-bearing rocks

We interpret peak *P–T* conditions of 16 kbar and 750 °C for 1.9 Ga eclogite facies metamorphism in the

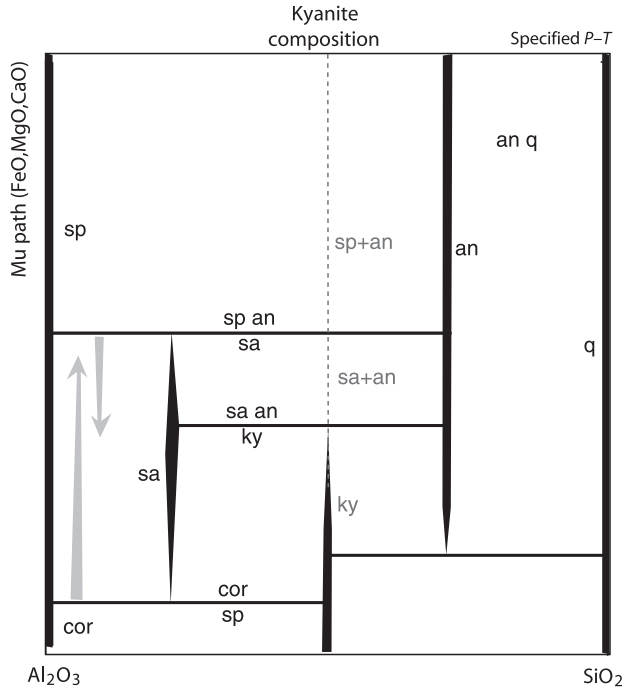

Fig. 15. Sketch of chemical potential path *v.* composition showing symplectite assemblages predicted to develop between kyanite and quartz depending on the chemical potentials of FeO, MgO and CaO. Reactions present can be seen by following paths shown on Figs 12 and 13. Dashed grey line indicates development of sa + an adjacent to kyanite, with development of sp + an distal to kyanite (crossing of sa + sp = an reaction shown in Fig. 13). Grey arrows indicate what would happen if the μ_{CaO} gradient were decreased, removing sapphirine stability and instead stabilizing corundum + anorthite.

Southern domain of the East Athabasca region of the STZ. Quantitative constraints on the metamorphic temperatures are provided by new garnet–clinopyroxene thermometry using the calibration of Krogh Ravna (2000) and methodology of Carson & Powell (1997). Recognizing the strong upward bias in temperature that results from assuming zero Fe^{3+}, the temperature estimate of 750 °C is significantly lower than that reported by Baldwin *et al.* (2004) for the same rocks (920–1000 °C). In addition, it is important to note that minimum uncertainties on the temperatures are ± 80 °C. To corroborate these results, Ti-in-zircon and Zr-in-rutile estimates of temperature were also obtained.

The Ti-in-zircon and Zr-in-rutile thermometers are potentially a more robust means of determining metamorphic temperatures, if zircon and/or rutile can be linked petrographically to metamorphic reactions or conditions. In this study, measurements were obtained from 1.9 Ga zircon inclusions in Na-clinopyroxene dated by SHRIMP (Baldwin *et al.*, 2004), and rutile inclusions in garnet. The results produced a narrow range of temperatures [720 ± 30 °C (zircon) and 797 ± 34 °C (rutile)], which is consistent with our estimate of ~750 °C for the maximum metamorphic temperature based on garnet–clinopyroxene thermometry. These independent sets of data require a revision in the previous higher temperature estimates.

Calculated pseudosections provide constraints on maximum pressures as well as the retrograde history of the eclogite. Pressure constraints are provided from *P–T* pseudosections contoured for plagioclase composition. Minimum pressures are inferred to be 16 kbar based on the jadeite content of clinopyroxene as well as the most sodic composition of retrograde plagioclase preserved in the rocks. This is less than the 18–20 kbar reported by Baldwin *et al.* (2004) because of the lower temperature now adopted. An important observation is that the pseudosections predict the stability of amphibole under eclogite facies conditions for both H_2O-saturated and H_2O-undersaturated bulk compositions. This is consistent with the observed mineral assemblages. Large pargasitic amphibole grains are present in many samples, which may have formed along the prograde path and persisted during peak metamorphism. The compositions preserved, however, indicate re-equilibration at lower pressure conditions as the large primary grains have similar compositions to that of the kelyphite rims surrounding garnet. The best estimate of pressure for the development and/or equilibration of pargasite along the retrograde path is 12–14 kbar at 750 °C.

Orthopyroxene coexists with plagioclase in symplectites, which is limited to maximum pressures of ~10 kbar, indicating that such symplectite formation may have occurred at lower *P–T* conditions compared to the amphibole-bearing symplectites. Plagioclase composition differs greatly between kelyphites around garnet (more calcic plagioclase) and orthopyroxene–plagioclase symplectites around clinopyroxene (more sodic plagioclase). Both these textures imply significant decompression, in the order of 15–20 km, based primarily on the maximum pressure stability of orthopyroxene.

The vein textures, where kyanite is layered with orthopyroxene, garnet, and plagioclase probably formed at maximum pressures of ~10 kbar, but still within kyanite stability. The formation of this layered structure may have involved a slowing in exhumation following a first phase of more rapid decompression. This would give sufficient time for such layering to develop, as well as the orthopyroxene–plagioclase symplectites that formed within the eclogite itself, which are interpreted to have formed at similar *P–T* conditions. Following the development of the layered vein structure, widespread development of symplectite textures resulted during a second phase of exhumation to mid-crustal depths.

Sapphirine-bearing rocks provide *P–T* constraints on the final decompression conditions recorded in the Southern domain. Because sapphirine–plagioclase and spinel–plagioclase textures cannot be modelled using a standard pseudosection approach as they are open system reaction textures, calculated petrogenetic grids

were used with fixed chemical potentials as a means to represent such equilibria. This method provides general *P–T* constraints on the development of sapphirine–plagioclase and spinel–plagioclase symplectites of 750 °C and 7 kbar. These *P–T* conditions are significantly lower than those previously inferred for such decompression textures in kyanite eclogites (Möller, 1999; Rötzler & Romer, 2001).

The *P–T* path that emerges from the synthesis of these data is shown in Fig. 16. This path is drawn to be isothermal at 750 °C with decompression conditions recorded at various stages following the peak conditions at ~16 kbar. Point 1 shows the *P–T* conditions of kelyphite formation, point 2 shows maximum orthopyroxene stability, just below which a hiatus in exhumation may have allowed time for widespread development of orthopyroxene-bearing textures in the eclogite, and finally, point 3, with the development of the sapphirine-bearing vein and reaction textures at mid-crustal depths. This *P–T* path will be framed within a temporal context next.

Timing constraints on the *P–T* path

The geochronological and thermochronological constraints available for the Southern domain eclogite are presented in Baldwin *et al.* (2004) and Flowers *et al.* (2006b). Zircon records two stages of growth, at 2.54 Ga and 1904 Ma (Baldwin *et al.*, 2004). The latter date has been linked to the eclogite facies metamorphism based on *in situ* dating zircon included in clinopyroxene (Baldwin *et al.*, 2004). The earlier date has not been linked to specific *P–T* conditions; it may reflect the protolith crystallization age, or an earlier high-grade metamorphic event in these rocks. Mafic granulites in the Southern domain also record 2.55–2.52 Ga and 1.9 Ga zircon dates (Baldwin *et al.*, 2003), and the host felsic gneiss records zircon and monazite growth at 2.6 and 1.9 Ga (Baldwin *et al.*, 2006). The difficulty in seeing through the 1.9 Ga high-*P* event to ascertain the Archean evolution of these rocks is clear, although inclusion patterns in garnet (zoisite + kyanite) and bulk geochemical data suggest that the eclogites were derived from plagioclase-bearing protoliths of troctolitic gabbro that crystallized at pressures ≤10 kbar (Baldwin *et al.*, 2004). There is no petrological evidence for an earlier lower pressure metamorphic event in the eclogite, only prograde growth of zoisite and pargasitic amphibole, as well as breakdown of plagioclase, on the way to higher pressure.

The cooling history of the Southern domain is well constrained, based on a variety of U–Pb thermochronometers. Titanite cooling ages reported from mafic granulites in the Southern domain are 1900–1894 Ma (Baldwin *et al.*, 2003). In the eclogite unit, rutile records cooling ages of 1.88–1.85 Ga (Baldwin *et al.*, 2004) and apatite cooling ages are 1.88–1.86 Ga (Flowers *et al.*, 2006b). Given the *P–T* path deduced

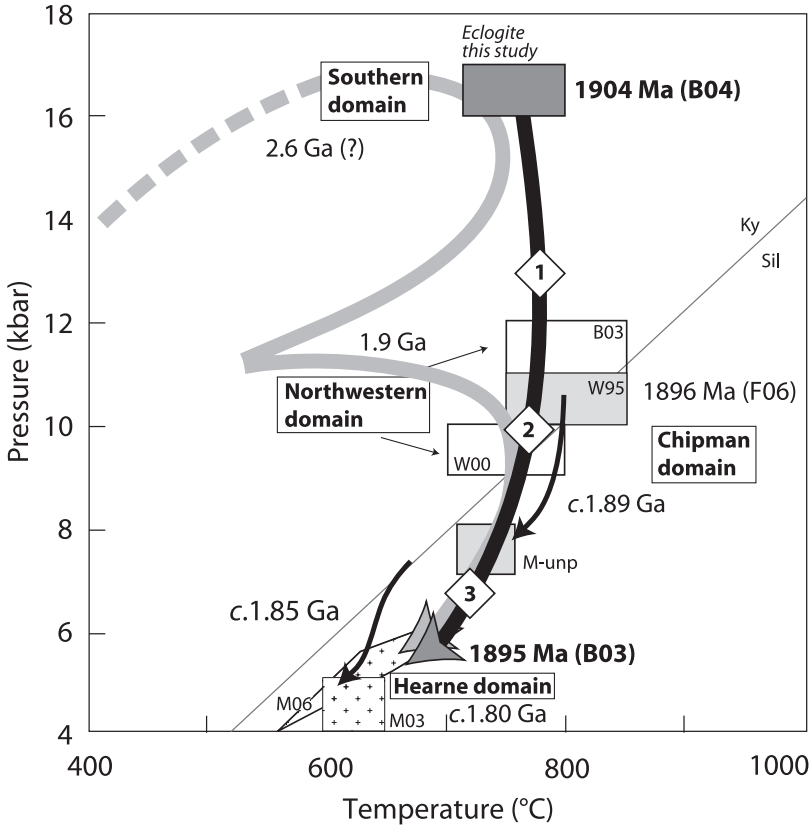

Fig. 16. *P–T* diagram for East Athabasca region. Two alternate *P–T* paths are presented. The heavy grey line shows two superimposed metamorphic events at 2.6 and 1.9 Ga, with cooling at residence at 10–12 kbar following the first event. This path is based on the preservation of Archean ages in all lithologies that might reflect an early high-grade metamorphic event. The heavy black arrow shows an alternate and preferred *P–T* path for the Southern domain based on the eclogite geochronology. Peak conditions of 16 kbar and 750 °C occurred at 1904 Ma [B04 – Baldwin *et al.* (2004)]. Numbers in diamonds indicate reaction texture constraints on the *P–T* path: 1, pargasite–plagioclase kelyphite; 2, orthopyroxene development in eclogite and sapphirine granulites; 3, sapphirine–spinel–plagioclase symplectites. Decompression took place over a *c.* 10 Myr interval by 1895 Ma based on titanite cooling ages [B03 – Baldwin *et al.* (2003)]. *P–T–t* paths for other domains are shown for comparison. Chipman domain (light grey boxes) (peak-W95 – Williams *et al.*, 1995; retrograde-M-unp – Mahan, unpublished data). Timing constraints from F06 (Flowers *et al.*, 2006a,b). North-western domain (peak-B03 and W00 – Williams *et al.*, 2000; Baldwin *et al.*, 2003). Hearne domain (footwall peak-M03 – Mahan *et al.*, 2003; hangingwall retrograde-M06 – Mahan *et al.*, 2006a).

above, with exhumation occurring isothermally at ~750 °C, the maximum amount of time for decompression of the eclogite from 16 kbar to ≤7.5 kbar is constrained by the titanite ages at 5–10 Myr. Thus ~25 km of exhumation occurred over this time interval, yielding rapid unroofing rates of 2.5–5 km Myr^{-1}. Based on the petrological evidence described above, this exhumation event may have occurred in two stages, first from 16 to 9–10 kbar and then finally to 7–8 kbar. Following rapid exhumation to mid-crustal depths, the rocks underwent a period of protracted cooling prior to a final phase of exhumation during regional contractional uplift related to the 1.85 Ga Legs Lake shear zone (Mahan *et al.*, 2003, 2006b; Flowers *et al.*, 2006b).

A comparison of *P–T* paths from each of the lithotectonic domains in the East Athabasca region is shown in Fig. 16. Two possible *P–T* paths are presented, the first is based largely on the geochronology of the eclogite, with high-*P* metamorphism occurring at 1.9 Ga (black line). An alternate *P–T* path based on the geochronology of the host felsic gneiss shows two superimposed high-grade events, at 2.6 and 1.9 Ga (grey line). The best-constrained segment of the Paleoproterozoic *P–T–t* path comes from data from the Chipman domain, where the 1896 Ma Chipman mafic dyke swarm occurs (Williams *et al.*, 1995; Flowers *et al.*, 2006a,b). In comparison with this domain, it is apparent that the Southern domain records higher pressures (16 kbar compared with 10–12 kbar), and at a slightly earlier time than the Chipman domain. In fact, exhumation of the Southern domain to mid-crustal levels was likely coincident in time with the 10–12 kbar metamorphism in the Chipman domain. The *c.* 8 Myr time interval between episodes of high-grade metamorphism is probably significant from a regional tectonic perspective. It is possible that the hiatus in exhumation in the Southern domain correlates with the high-*P* metamorphism within the adjacent Chipman domain, marking a shift from a regional compressional regime (when the eclogite formed) and the onset of extensive mafic magmatism in the Chipman domain during extension and regional underplating appear to be related. The two domains appear to share a common *P–T–t* history following the initial phase of rapid decompression, but the Southern domain does not record evidence for the widespread mafic magmatism that affected the Chipman domain. Therefore, it is likely that ultimate juxtaposition of these domains occurred following this underplating event, and certainly the two terranes shared a common exhumation history by 1.85 Ga during regional contractional uplift along the Legs Lake shear zone (Mahan *et al.*, 2003, 2006b; Flowers *et al.*, 2006b).

The heterogeneous nature of exhumation amongst the different domains is clear, with the Southern domain recording distinctly deeper crustal level exposures as well as the oldest period of high-*P* metamorphism. The revised temperatures presented here are more compatible with the emerging story for the metamorphic evolution of the granulites of the East Athabasca region. Temperatures of ~750 °C in the Southern domain do not require a 'mantle' heat source for metamorphism, and thus are consistent with them simply being more deeply exhumed than the surrounding domains. The older age of metamorphism preserved in the Southern domain is consistent with the eclogite facies metamorphism being a result of shortening and thickening prior to the onset of regional unroofing associated with widespread mafic magmatism. Thus the eclogites of the Southern domain are an important key to unravelling the tectonic scenario that resulted in the ultimate exhumation of this deep crustal terrane.

CONCLUSIONS

New petrological data from eclogites from the Southern domain of the East Athabasca region suggest peak conditions of 16 kbar and 750 °C, with no evidence for ultrahigh-temperature conditions. Peak conditions were followed by isothermal decompression to ~7 kbar, reflected in a spectacular range of reaction textures, particularly involving sapphirine- and spinel-bearing symplectites that occur associated with kyanite breakdown, in veins and in rocks marginal to the eclogite unit. The youngest decompression segment is constrained using phase diagrams calculated with fixed chemical potentials, which is a new approach for examining open-system reaction textures such as these. These results suggest that the entire early unroofing segment that exhumed rocks from ~50 to 25 km crustal depths occurred between 1904 and 1894 Ma. This time interval precedes regional unroofing in the other domains of the East Athabasca region and marks the onset of regional extension that perhaps drove widespread mafic magmatism in the other domains. Following this rapid decompression, the rocks resided at mid-crustal depths until ultimately being exhumed by regional contraction along the Legs Lake shear zone at 1.85–1.80 Ga.

ACKNOWLEDGEMENTS

This research was supported by National Science Foundation grant EAR-0001131 to S. Bowring and M. Williams, as well as an NSF graduate research fellowship to J.B. R.P. acknowledges support of ARC DP0451770, and the hospitality of ETH (Zurich) where R.P. and J.B. initiated some methodological aspects of this work in 2004. J.B. acknowledges support of NSF-EAR-02275553 and the University of Maryland. We thank R. White for helpful discussions, B. McDonough for assistance with zircon LA-ICP-MS analysis and M. Jercinovic for assistance with the rutile microprobe analysis. Reviews by A. Proyer and C. Warren greatly improved the clarity of the manuscript.

REFERENCES

Baldwin, J. A., Bowring, S. A. & Williams, M. L., 2003. Petrological and geochronological constraints on high pressure, high temperature metamorphism in the Snowbird tectonic zone, Canada. *Journal of Metamorphic Geology*, **21,** 81–98.

Baldwin, J. A., Bowring, S. A., Williams, M. L. & Williams, I. S., 2004. Eclogites of the Snowbird tectonic zone: petrological and U-Pb geochronological evidence for Paleoproterozoic high-pressure metamorphism in the western Canadian Shield. *Contributions to Mineralogy and Petrology*, **147,** 528–548.

Baldwin, J. A., Bowring, S. A., Williams, M. L. & Mahan, K. H., 2006. Geochronological constraints on the evolution of high-pressure felsic granulites from an integrated electron microprobe and ID-TIMS geochemical study. *Lithos*, **88,** 173–200.

Berman, R. G., Ryan, J. J., Tella, S. *et al*., 2000. *The Case of Multiple Metamorphic Events in the Western Churchill Province: Evidence from Linked Thermobarometric Data, and Jury Deliberations*. Geological Association of Canada – Mineralogical Association of Canada Annual Meeting, Calgary, Alberta. Abstracts on CD-ROM.

Carson, C. J. & Powell, R., 1997. Garnet-orthopyroxene geothermometry and geobarometry: error propagation and equilibration effects. *Journal of Metamorphic Geology*, **15,** 679–686.

Carswell, D. A., Möller, C. & O'Brien, P. J., 1989. Origin of sapphirine-plagioclase symplectites in metabasites from Mitterbachgraben Dunkelsteinerwald granulite complex, Lower Austria. *European Journal of Mineralogy*, **1,** 455–466.

Cherniak, D. J., Manchester, J. & Watson, E. B., 2007. Zr and Hf diffusion in rutile. *Earth and Planetary Science Letters*, doi: 10.1016/j.epsl.2007.06.027, (in press).

Dale, J., Powell, R., White, R. W., Elmer, F. L. & Holland, T. J. B., 2005. A thermodynamic model for Ca-Na clinoamphiboles in Na2O-CaO-FeO-MgO-Al2O3–SiO2–H2O–O for petrological calculations. *Journal of Metamorphic Geology*, **23,** 771–791.

Ferry, J. M. & Watson, E. B., 2007. New thermodynamic models and revised calibrations for the Ti-in-zircon and Zr-in-rutile thermometers. *Contributions to Mineralogy and Petrology*, doi: 10.1007/s00410-007-0201-0, (in press).

Flowers, R. M., Bowring, S. A. & Williams, M. L., 2006a. Timescales and significance of high-pressure, high-temperature metamorphism and mafic dike anatexis, Snowbird tectonic zone, Canada. *Contributions to Mineralogy and Petrology*, **151,** 558–581.

Flowers, R. M., Mahan, K. H., Bowring, S. A., Williams, M. L., Pringle, M. S. & Hodges, K. V., 2006b. Multistage exhumation and juxtaposition of lower continental crust in the western Canadian Shield: linking high-resolution U-Pb and 40Ar/39Ar thermochronometry with pressure-temperature-deformation paths. *Tectonics*, **25,** TC4003, doi:10.1029/2005TC001912.

Goodacre, A. K., Grieve, R. A. F., Halpenny, J. F. & Sharpton, V. L., 1987. *Horizontal Gradient of the Bouguer Gravity Anomaly Map of Canada, Canadian Geophysical Atlas, Map 5*. Geological Survey of Canada, Ottawa.

Hanmer, S., 1994. Geology, East Athabasca mylonite triangle, Stony Rapids area, northern Saskatchewan. In: *Geological Survey of Canada Map 1859A* Scale 1:100,000.

Hanmer, S., 1997. Geology of the Striding-Athabasca mylonite zone, northern Saskatchewan and southeastern District of Mackenzie, Northwest Territories. *Geological Survey of Canada Bulletin*, **501,** 1–92.

Hanmer, S., Parrish, R., Williams, M. & Kopf, C., 1994. Striding-Athabasca mylonite zone: complex Archean deep-crustal deformation in the East Athabasca mylonite triangle, northern Saskatchewan. *Canadian Journal of Earth Sciences*, **31,** 1287–1300.

Hanmer, S., Williams, M. & Kopf, C., 1995a. Modest movements, spectacular fabrics in an intracontinental deep-crustal strike-slip fault: striding-Athabasca mylonite zone, NW Canadian Shield. *Journal of Structural Geology*, **17,** 493–507.

Hanmer, S., Williams, M. & Kopf, C., 1995b. Striding-Athabasca mylonite zone: implications for the Archean and Early Proterozoic tectonics of the western Canadian Shield. *Canadian Journal of Earth Sciences*, **32,** 178–196.

Hoffman, P. F., 1988. United Plates of America, the birth of a craton: Early Proterozoic assembly and the growth of Laurentia. *Annual Reviews of Earth and Planetary Science Letters*, **16,** 543–603.

Hoffman, P. F., 1989. Precambrian geology and tectonic history of North America. In: *The Geology of North America – An Overview* (eds Bally, A.W. & Palmer, A.R.), pp. 447–512. Geological Society of America, Boulder, CO.

Holland, T. J. B., 1980. The reaction albite = jadeite + quartz determined experimentally in the range 600–1200 °C. *American Mineralogist*, **65,** 129–134.

Holland, T. J. B. & Powell, R., 1996. Thermodynamics of order-disorder in minerals 2: symmetric formalism applied to solid solutions. *American Mineralogist*, **81,** 1425–1437.

Holland, T. J. B. & Powell, R., 1998. An internally-consistent thermodynamic data set for phases of petrological interest. *Journal of Metamorphic Geology*, **16,** 309–343.

Holland, T. J. B. & Powell, R., 2003. Activity-composition relations for phases in petrological calculations: an asymmetric multicomponent formulation. *Contributions to Mineralogy and Petrology*, **145,** 492–501.

Johansson, L. & Möller, C., 1986. Formation of sapphirine during retrogression of a basic high-pressure granulite, Roan, Western Gneiss Region, Norway. *Contributions to Mineralogy and Petrology*, **94,** 29–41.

Korzhinskii, D. S., 1957. *Physico-Chemical Basis for the Analysis of the Paragenesis of Minerals*. Nauka, Moscow.

Krogh Ravna, E. J., 2000. The garnet-clinopyroxene Fe2 + -Mg geothermometer: an updated calibration. *Journal of Metamorphic Geology*, **18,** 211–219.

Krogh Ravna, E. J. & Terry, M. P., 2004. Geothermobarometry of UHP and HP eclogites and schists – an evaluation of equilibria among garnet-clinopyroxene-kyanite-phengite-coesite/quartz. *Journal of Metamorphic Geology*, **22,** 579–592.

Liati, A. & Seidel, E., 1994. Sapphirine and högbomite in overprinted kyanite-eclogites of central Rhodope, N. Greece: first evidence of granulite facies metamorphism. *European Journal of Mineralogy*, **6,** 733–738.

Mahan, K. H. & Williams, M. L., 2005. Reconstruction of a large deep-crustal terrane: implications for the Snowbird tectonic zone and early growth of Laurentia. *Geology*, **33,** 385–388.

Mahan, K. H., Williams, M. L. & Baldwin, J. A., 2003. Contractional uplift of deep crustal rocks along the Legs Lake shear zone, western Churchill Province, Canadian Shield. *Canadian Journal of Earth Sciences*, **40,** 1085–1110.

Mahan, K. H., Goncalves, P., Williams, M. L. & Jercinovic, M. J., 2006a. Dating metamorphic reactions and fluid flow: application to exhumation of high-P granulites in a crustal scale shear zone, western Canadian Shield. *Journal of Metamorphic Geology*, **24,** 193–217.

Mahan, K. H., Williams, M. L., Flowers, R. M., Jercinovic, M. J., Baldwin, J. A. & Bowring, S. A., 2006b. Geochronological constraints on the Legs Lake shear zone with implications for regional exhumation of lower continental crust, western Churchill Province, Canadian Shield. *Contributions to Mineralogy and Petrology*, **152,** 223–242.

Möller, C., 1999. Sapphirine in SW Sweden: a record of Svecnorwegian (-Grenvillian) late-orogenic tectonic exhumation. *Journal of Metamorphic Geology*, **17,** 127–141.

O'Brien, P. J., 1992. The formation of sapphirine and orthopyroxene during overprinting of Mariánské Lázne

Complex eclogites.. *Zentralblatt für Geologie und Paläontologie* **(7/8),** 827–836.
O'Brien, P. J. & Rötzler, J., 2003. High-pressure granulites: formation, recovery of peak conditions and implications for tectonics. *Journal of Metamorphic Geology*, **21,** 3–20.
Powell, R., 1985. Regression diagnostics and robust regression in geothermometer/geobarometer calibration: the garnet-clinopyroxene geothermometer revisited. *Journal of Metamorphic Geology*, **3,** 231–243.
Powell, R., Holland, T. J. B. & Worley, B., 1998. Calculating phase diagrams involving solid solutions via non-linear equations, with examples using THERMOCALC. *Journal of Metamorphic Geology*, **6,** 173–204.
Powell, R., Guiraud, M. & White, R. W., 2005. Truth and beauty in metamorphic phase-equilibria: conjugate variables and phase diagrams. *Canadian Mineralogist*, **43,** 21–33.
Proyer, A., Dachs, E. & McCammon, C., 2004. Pitfalls in geothermobarometry of eclogites: Fe^{3+} and changes in the mineral chemistry of omphacite at ultrahigh pressures. *Contributions to Mineralogy and Petrology*, **147,** 305–318.
Rötzler, J. & Romer, R. L., 2001. P-T-t evolution of ultrahigh-temperature granulites from the Saxon Granulite Massif, Germany. Part I: Petrology. *Journal of Petrology*, **42,** 1995–2013.
Snoeyenbos, D. R., Williams, M. L. & Hanmer, S., 1995. Archean high-pressure metamorphism in the western Canadian Shield. *European Journal of Mineralogy*, **7,** 1251–1272.
Stipska, P. & Powell, R., 2005a. Constraining the *P–T* path of a MORB-type eclogite using pseudosections, garnet zoning and garnet–clinopyroxene thermometry: an example from the Bohemian Massif. *Journal of Metamorphic Geology*, **23,** 725–743.
Stipska, P. & Powell, R., 2005b. Does ternary feldspar constrain the metamorphic conditions of high-grade metaigneous rocks? Evidence from orthopyroxene gneisses, Bohemian Massif. *Journal of Metamorphic Geology*, **23,** 627–647.
Tomkins, H. S., Powell, R. & Ellis, D. J., 2007. The pressure dependence of the zirconium-in-rutile thermometer. *Journal of Metamorphic Geology*, **25,** 703–713.
Watson, E. B. & Harrison, T. M., 2005. Zircon thermometer reveals minimum melting conditions on earliest earth. *Science*, **308,** 841–844.
Watson, E. B., Wark, D. A. & Thomas, J. B., 2006. Crystallization thermometers for zircon and rutile. *Contributions to Mineralogy and Petrology*, **151,** 413–433.
White, R. W., Powell, R. & Holland, T. J. B., 2001. Calculation of partial melting equilibria in the system Na_2O-CaO-K_2O-FeO-MgO-Al_2O_3-SiO_2-H_2O (NCKFMASH). *Journal of Metamorphic Geology*, **19,** 139–153.
Williams, M. L., Hanmer, S., Kopf, C. & Darrach, M., 1995. Syntectonic generation and segregation of tonalitic melts from amphibolite dikes in the lower crust, Striding-Athabasca mylonite zone, northern Saskatchewan. *Journal of Geophysical Research*, **100,** 15717–15734.
Williams, M. L., Melis, E. A., Kopf, C. & Hanmer, S., 2000. Microstructural tectonometamorphic processes and the development of gneissic layering: a mechanism for metamorphic segregation. *Journal of Metamorphic Geology*, **18,** 41–57.

Received 5 February 2007; revision accepted 1 August 2007.